Mapping urban fabric for enhanced urban climate modelling based on a historical building classification

Bianca E. Sandvik[1], Dragan Milošević[1,2], and Gert-Jan Steeneveld[1]

[1]Meteorology and Air Quality Section, Wageningen University, Wageningen, 6708PB, The Netherlands
[2]Hydrology and Environmental Hydraulics Section, Wageningen University, Wageningen, 6708PB, The Netherlands

Correspondence to: Bianca E. Sandvik (bianca.sandvik@wur.nl)

Abstract

The urban climate conditions are heavily influenced by the morphological and thermal properties of buildings. Recent studies have been focussed on the representation of urban morphology using standardised Local Climate Zones (LCZs) whereas relatively little research has been performed on the impact of thermal properties of buildings. Though useful for categorising and modelling urban climates, generic LCZ classes can have a low representativeness for local spatial heterogeneity while also not accounting for variations in building thermal properties.

Using Amsterdam (the Netherlands) as a case study, we develop an alternative classification of urban fabric based on construction period, historical construction practices and regulations. This HERITAGE classification consists of 10 distinct classes which we combine with 3D building model data, the Dutch cadastre and previous studies using GIS to derive their accompanying morphological traits. This approach offers a new method to create literature- and data-based urban classes with customised spatially varying morphological and thermal parameter values which are more representative of the real world compared to the LCZ approach. The HERITAGE-classes contain all necessary variables for conducting thermal and energy assessments as well as numerical modelling of the urban climate using for example the Weather Research and Forecasting (WRF) model.

1 Introduction

The urban climate is affected by the complex processes at hand. A building interacts with neighbouring buildings and streets through energy gain and loss depending on occupancy behaviour, heating and cooling devices – and the prevailing weather and climate conditions. The heat exchange between a building and the environment depends on the buildings shape, its material composition and placement, insulation, orientation, and relation to other objects. These governing factors are what researchers, architects and spatial planners adjust in optimising indoor and outdoor urban spaces for thermal comfort, climate change mitigation and aesthetics.

When buildings amass into urban areas, they can significantly modify the local energy and radiation balance compared to rural areas (Oke et al., 2017). Due to the concentration of material and people, together with trapping of radiation between structures, heat tends to accumulate and store longer in urban areas compared to rural counterparts. This phenomenon is most known as the Urban Heat Island (UHI) effect and is a subject of continuous study within urban meteorology and climate research (Bahadori et al., 2025; Cheval et al., 2024).

Historically the options for modifying urban environments have encountered restrictions. Availability of space, financial resources, construction materials, technological advances, local climatological adaptations and building regulations are among factors that affect historical and contemporary building construction. This may lead to different neighbourhoods within the same city to have completely different characteristics with regards to aesthetical, morphological and thermal properties, which may again affect the local- and micro-climate conditions. Capturing this heterogeneity of urban characteristics remains a challenge for multiple research fields such as meteorology, hydrology, remote sensing, architecture, spatial planning, public health and energy demand (Cheng et al., 2025; Esch et al., 2022; Li et al., 2024; Lindenthal and Johnson, 2025; Masson et al., 2020; TABULA Project Team, 2012). Better insight into urban complexity helps us understand what makes a place desirable to live in, how the area functions and how to improve the living conditions over time.

Earlier studies have attempted to systematically describe the urban environment with increasing granularity. In an attempt to standardise descriptions of urban environments, Stewart and Oke (2012) developed a framework of Local Climate Zones (LCZs) to facilitate comparison of urban environments and simplify descriptions of climate measurement sites. This framework has been widely adopted both within and outside the climate research community to assess the impact of a city's *standardised morphology* on topics such as local climate and meteorology, urban design and planning, pollution, human health and building energy use (Han et al., 2024; Huang et al., 2023).

Stewart and Oke (2012) defined ten LCZ classes that can be grouped into four categories of surface properties: surface structure, surface cover, surface material and human activity. Initial efforts to classify individual cities into LCZs have over time grown into the development of global and continental maps through the WUDAPT-project (Brousse et al., 2016; Demuzere et al., 2019, 2022). Despite the versatility of the LCZ approach its generalisability has its use limits. In a large review of LCZ mapping, Huang et al. (2023) found that, of the four categories of surface properties, mainly surface structure and surface cover have been used for LCZ classification methods. Whereas – despite their potential importance for characterising the urban environment – "surface material and human activity are rarely employed due to a lack of data". Parameters of surface materials are usually considering only albedo and emissivity and are commonly taken from conventional LCZ tables provided by e.g. Stewart and Oke (2012).

The choice of surface material affects the thermal properties of the surface which again affect the energy balance of the surface through a change in albedo, emissivity and thermal storage capacity. In the context of modelling building energy fluxes, it is important to know the thermal properties of an entire facet (aka. the walls and roof) to properly quantify the energy transfer between the indoor and outdoor environment. To estimate this as accurately as possible, it is critical to know how the building is constructed and its building materials. Despite this knowledge, there has been limited research efforts going into categorising urban environments based on primarily thermal aspects instead of morphological aspects.

Tornay et al. (2017, hereafter T17) developed 10 building archetypes based on building morphology, construction period and materials, building use and geographical location for France and assessed the sensitivity of the Town Energy Balance model (Masson, 2000) to these archetypes and their properties. They found especially roof albedo, presence and thickness of insulation material and its position in the facet to strongly affect the urban energy balance through modifying the radiation balance and thermal storage. Buildings with slate roofs showed higher values of net radiation, sensible heat flux, indoor temperatures and higher amplitudes in diurnal heat storage compared to buildings with roofs of zinc and tiles in their summer simulations. They also found that the relative importance of building wall material to roof material increases with building density. Walls with lower thermal conductivity stored less heat but showed higher sensible heat flux compared to highly thermal conductive wall materials. During winter, they found only a 10 % variation in heating demand between material setups because wall materials with larger thermal conductivity tended to be thicker. When comparing construction periods, they found a generally decreasing trend in heat energy consumption and sensible heat flux with increasing building year during winter due to increased insulation. Interestingly, their oldest (<1949) and most recent (>2012) construction periods showed comparable low values for stored sensible heat and similar diurnal variability for sensible heat flux which they attributed to lack of concrete under the roof tiles and external placement of insulation material, respectively.

In order to couple buildings to specific energy consumption load curves, Pappaccogli et al. (2021) categorised buildings in Bolzano, Italy into four building classes: non-residential, hospitality, and residential buildings before and after 1978. They found that buildings constructed before 1978 had a higher morning peak energy load but a lower energy load in the evening across multiple seasons. For their WRF model simulations they used three building classes (high- and low-energy consumption residential, and industrial/commercial), but both residential classes had the same thermal properties. They hypothesised the model's overestimation and underestimation of energy consumption during peaks and mid-day hours respectively could be caused by an incorrect definition of thermal properties of the buildings.

Aksoezen et al. (2015) studied links between measured energy consumption and building properties in Basel, Switzerland. They grouped and analysed buildings based on four periods of construction and found that building volume, gross floor area, compactness and building age affect energy demand. As expected, larger buildings lead to higher energy demand. The authors found compactness (building surface area to volume ratio) to be significantly negatively correlated (-0.6) to building age and significantly positively correlated (+0.3) to energy demand. Surprisingly they also found that the connection between energy demand and building age was not linear with time, but concave. They found that buildings constructed before 1921 have lower energy demand than buildings constructed in the following six decades. Like Huang et al. (2023), they acknowledged that a key limitation of using general building typologies connected to the lack of data on material composition and refurbishments, especially for older buildings.

To summarise: previous urban studies have overwhelmingly focused on morphological building parameters to quantify the environmental impacts of the urban environment due to a lack of data on thermal properties of buildings. A limited number of previous studies have focused on the impacts of the construction period on the

surface energy balance and energy consumption and found them to be non-linear with time due to changes in materials and construction practices. All these findings demonstrate the importance of properly accounting for the thermal properties of buildings in urban energy modelling in order to fully assess their current and future impact on the environment and society. However, it remains unclear how age-dependent building properties affect urban climate modelling.

Therefore, our research question is: *what is the impact of spatially varying thermal and morphological properties based on historical building construction on the local meteorology and climate?*

Hence, we introduce a novel methodology for categorising buildings and neighbourhoods into distinct classes based on building period. We demonstrate the approach for Amsterdam, the Netherlands, linking historical construction practices and materials to building periods, 3D building data and road data. This results in 10 HERITAGE-classes that contain variables suitable for conducting thermal and energy assessments and modelling of the urban environment using numerical models such as WRF (Chen et al., 2011) and PALM4U (Maronga et al., 2020).

2 Data and methods

This section explains the methodology for creating the 10 HERITAGE-classes (HCs) and the data sourced for this purpose (Figure 1).

Amsterdam was selected as a testbed due to its historic expansion and variable building stock as well as the presence of long-term urban meteorological observations for model validation (Ronda et al., 2017). Resulting building parameter values are customised to fit the inner city of Amsterdam but is also representative for similarly constructed Dutch cities. Despite differences in regional historical construction, we consider the resulting thermal parameter values to be fairly representative for the Netherlands as a whole. Contrarily, differences in morphological parameters can vary strongly between cities and are recommended to be tailored to the area of interest.

Creating spatial datasets for categorisation of urban environments require information on five major parameter groups: land use and land cover, morphological parameters, architectural parameters, socio-economic parameters and building use, and urban vegetation. The main approaches for creating spatial datasets are either based on remote sensing techniques or GIS approaches, or a combination of the two. For a thorough overview of needs and sources from a LCZ perspective see Masson et al. (2020). This current work aggregates multiple mainly existing GIS and remote sensing data sources.

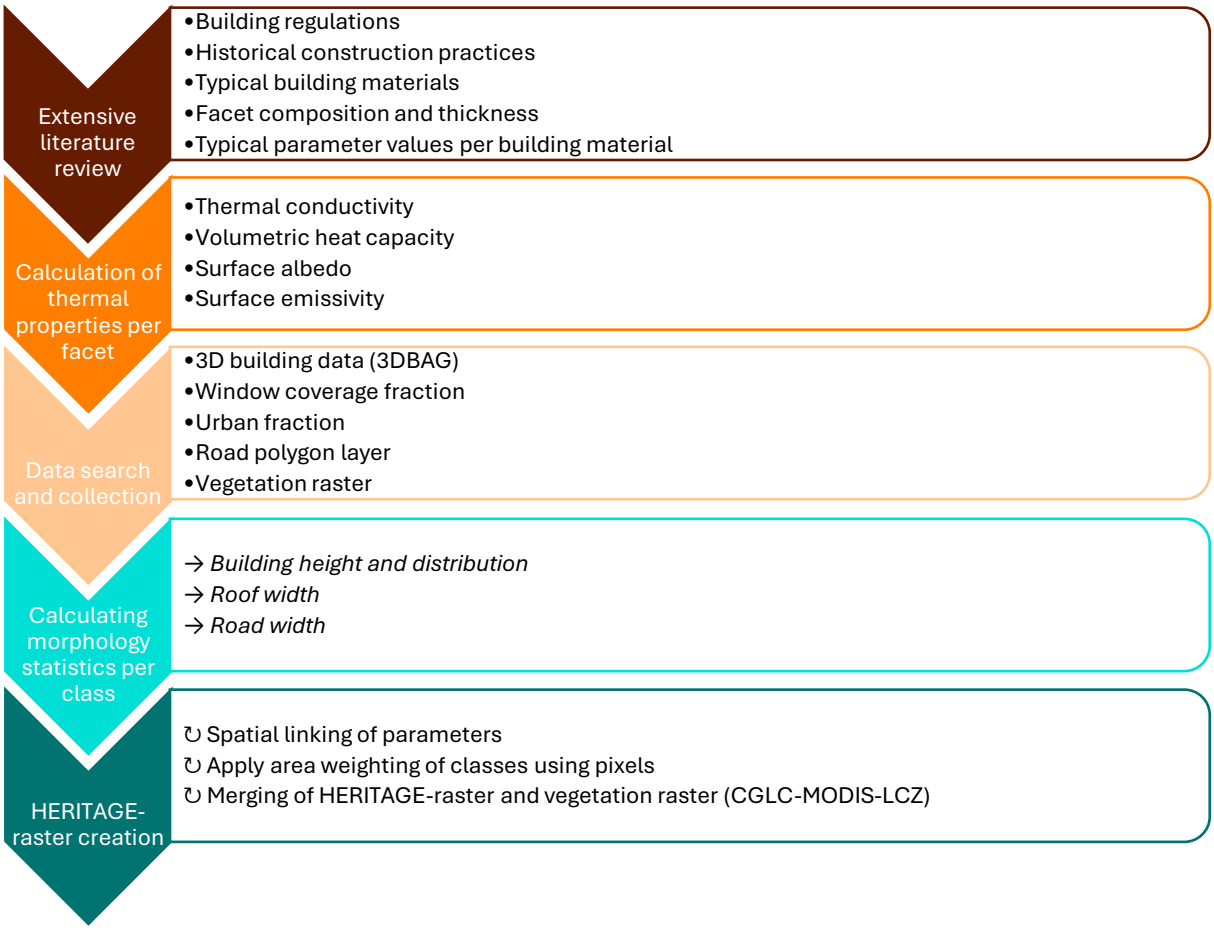


Figure 1: Simplified workflow diagram for developing the HERITAGE-classes and HERITAGE-raster with input sources (•), outcomes (→), and processes (↻).

2.1 Data collection

2.1.1 Sourcing thermal properties

We start with an extensive literature review to identify building periods that are distinctly different in terms of thermal properties of buildings. We combine documentation on historical building construction practices and archetypes, and historical building regulations. Subsequently, 19 building periods were identified based on typical building construction factors, such as thickness and material composition of facets, presence of cavity walls and insulation, and changes in building regulations. In total, 28 different sources have been used consisting of journal articles, government reports and numerous diverse sources (Table A1).

Next, typical values of thermal properties for the identified materials were gathered and used to estimate representative values for thermal conductivity, specific heat capacity, surface albedo, and surface emissivity per facet and building period. In total, 13 different materials were identified, and their thermal property values were estimated based on nine different sources (Table A2). Finally, building periods with similar thermal property values were grouped resulting in 10 HCs with distinctly different thermal property values (Table 1 and 2).

Table 1: The 10 HERITAGE-classes with example buildings from Amsterdam (Google Streetview) and their occurrence within our area of interest as reported by 3DBAG.

HERITAGE 1 <1800	HERITAGE 2 1800–1929	HERITAGE 3 1930–1945	HERITAGE 4 1946–1964	HERITAGE 5 1965–1974
				
1.5 %	18.1 %	9.4 %	16.1 %	10.7 %

HERITAGE 6 1975–1991	HERITAGE 7 1992–2005	HERITAGE 8 2006–2014	HERITAGE 9 ≥2015	HERITAGE 10 Unknown (1005)
				
19.3 %	12.1 %	7.3 %	5.3 %	0.2 %

Values of surface albedo and surface emissivity of the HCs are mainly taken from reference lookup tables based on the outermost material listed for their respective facet composition (Table A2). Since windows can significantly affect the thermal transfer through walls, the window coverage fraction (aka. window-to-wall ratio) per period was taken from (Dang et al., 2024). The 10th HERITAGE-class "Unknown" (HC10) is based on – as Huang et al. (2023) pointed out – the fact that data on building year and construction often is lacking. All thermal property values for this "Unknown" class are the average of each parameter of all the other HCs. This allows all buildings to be categorised into a HERITAGE-class depending on their (un)known building year.

2.1.2 Sourcing morphological properties

The second step entails collecting multiple spatial datasets which were processed in QGIS before morphological values could be calculated per HERITAGE-class.

Extracting building polygons

Our approach is based on 3DBAG (v2024.12.16) – a 3D building dataset covering the whole of the Netherlands (Peters et al., 2022). The 3DBAG data have been generated based on the Dutch building cadastre and the National Digital Elevation Model of the Netherlands (AHN) which results in the 3D building model containing parameters such as building ID, original building year, height above sea level, roof type, ground floor area, volume, roof elevation and location. We extracted all building polygons for Level of Detail (LoD) 2.2 (Peters et al., 2022) in a rectangular area covering the whole city of Amsterdam through 3DBAGs WFS service in combination with QGIS version 3.34.

We first identified and then addressed two issues with the 3DBAG data: 1) each building may be composed of more than one polygon, and 2) the building heights come from AHN LiDAR data which need correction for the terrain height. To address these issues, we aggregated all polygons based on their building ID, multiplying the ground floor area and volume of the polygons together before calculating a new mean building height based on

the area weighted building height of the aggregated polygons. Subsequently we adjusted this area weighted mean building height by subtracting the height above sea level. Data attributes not needed were removed leaving a building layer with one polygon per building with attributes such as: building ID, area weighted mean building height, total ground floor area, volume, and original building year. We then grouped the building polygons into 10 separate QGIS layers based on their building year attribute according to the 10 HCs.

Extracting building heights and their distributions

Depending on the use case, different building height statistics need to be estimated. For relatively straightforward schemes, such as WRFs Single Layer Urban Canopy Model (SLUCM, Kusaka et al., 2001), mean and standard deviations were obtained through the use of zonal statistics directly in QGIS. For more advanced model schemes – such as BEP-BEM (Martilli et al., 2002; Salamanca et al., 2010) – requiring building height distributions, we calculated building height distributions in 5 m bins. The upper bin bound was selected based on the first occurrence below 10 % for each class. Manual adjustment was done by grouping unusually tall buildings into the highest building height category, rounding each bin to whole percentages, and ensuring the distribution added up to 100 %. Due to a highly right-skewed building height distribution caused by a disproportionate number of smaller entities (such as sheds, house boats, market stands and house expansions) in outer districts, this binning process was redone for a subset of buildings covering the inner-city of Amsterdam (4.87159˚E, 52.38677˚N, 4.92801˚E, 52.35809˚N). We chose to implement the inner-city building height distribution for the HCs because this distribution is less impacted by more rural and suburban building practices and thus better reflects the urban environment of Amsterdam. The resulting building height distributions per HC is presented in Table 3.

Extracting roof widths

Buildings in Amsterdam have typically a rectangular footprint with the shortest side facing the street (Peters et al., 2022). This feature is utilised when calculating the typical building roof width needed for representing the urban canyon for modelling applications. We first generate building "skeletons" with centerlines for all buildings using the Skeleton-tool from the BecaGIS plugin (Quach, 2024). We then calculate the length of the centerline and add this as a building attribute. To estimate the median roof width for each HC, we use QGISs built in zonal statistics. To be consistent for building morphology parameters, only the roof width values for buildings located in the inner-city domain was used for the HCs. The resulting median roof width estimates per HC are presented in Table 3.

Extracting road widths

The last morphological parameter to obtain is road width. This parameter were calculated based on the road area layer ("wegdeel_vlak") from the TOP10NL dataset provided by the Dutch cadastre (Kadaster, n.d.). To estimate the road width, we first extracted and merged all road polygons within our study area based on road name in order to avoid big roads being underestimated when they consist of multiple polygons. Thereafter, we calculated the length of the road polygons using the Skeleton-tool as outlined before for the roof width estimates and added this as an attribute to the polygons. The road width was calculated as the polygon area divided by its length and was added as an attribute field to each road polygon.

Next, we needed to calculate road statistics on neighbourhood level to align with the HCs. We calculated and transferred statistics on occurring building year and road width by joining neighbourhood polygons ("buurten") provided by the Centraal Bureau voor de Statistiek (2024) with attributes from the singular 3DBAG building layer and the road polygons from before. Subsequently, we allocated a HC to each neighbourhood using the field calculator with the criteria that both the mean and median calculated building year falls within a singular HC range (e.g. 1930–1945). If the criteria were not fulfilled the neighbourhood was allocated to the HERITAGE-class 10 (Unknown) (HC10). We set a requirement of at least one road and 10 buildings per neighbourhood polygon and excluded the rest as input for the final calculation of median road width per HERITAGE-class.

2.1.3 Sourcing vegetation and urban fraction

Two non-morphological properties were sourced from established sources: vegetation and urban fraction. To include vegetation and facilitate easy comparison between the LCZ and HERITAGE approaches, we based our vegetation data on the global CGLC-MODIS-LCZ dataset from Demuzere et al. (2023a), which is the default dataset in WRF. We extracted our region of interest and reclassified all LCZ-classes to "Bare rock/paved" (class 61) to remove the LCZs and avoid missing pixels when merging this modified CGLC-MODIS-LCZ raster with the HERITAGE-raster pixels after their generation outlined in Sect. 2.2 (Figure 2). Section 3.2 discloses the 19 natural landcover categories from CGLC-MODIS-LCZ and the differences between this default LCZ-raster and the HERITAGE-raster.

Urban fraction was estimated based on 30 m×30 m data from Ronda et al. (2017). We refined these data to even finer pixels of 1/3 of the original size and calculated the urban fraction by dividing the pixel colour value by the maximum colour value before spatially joining them to the HERITAGE class-pixels generated in the following section (Sect. 2.2). The final urban fraction values per HC were obtained using zonal statistics in QGIS and are available in Table 2.

2.2 Developing the HERITAGE-raster

We developed a HERITAGE-raster using 3DBAG and the modified CGLC-MODIS-LCZ based on area weighting using pixels in QGIS (Figure 2). We first created two HERITAGE-rasters with different pixel sizes from the original HERITAGE polygon layer created from 3DBAG in Sect. 2.1.2, where the largest match the grid of the CGLC-MODIS-LCZ raster (60 m×100 m) and the finest is 50 times finer (1.2 m×2 m). Secondly, we converted the raster pixels of both layers to polygons again and joined the attributes by location using majority as the discerning factor. This determines the most frequently occurring HERITAGE-class in the fine raster within each larger pixel; i.e. this approach creates an alternative area weighting technique using raster pixel sizes. Third, we converted the new generated pixel layer with the same grid size as CGLC-MODIS-LCZ to raster format. Finally, we merged the HERITAGE-raster with the modified CGLC-MODIS-LCZ vegetation raster from Sect. 2.1.3. This resulted in a HERITAGE-raster with CGLC-MODIS vegetation.

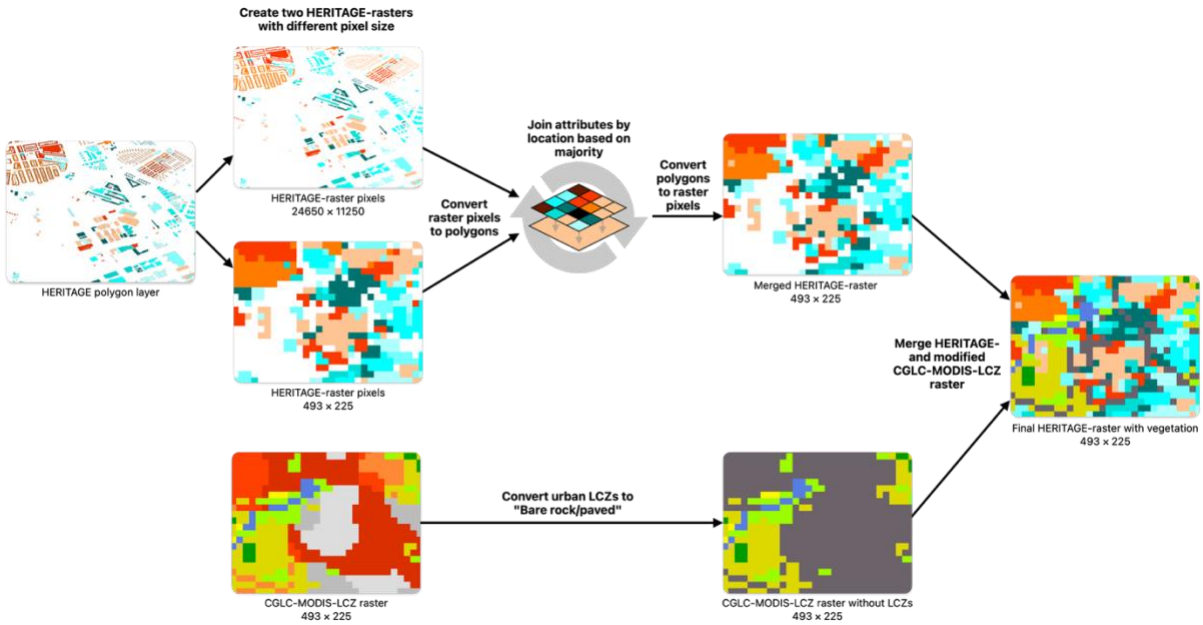


Figure 2: Illustration of the workflow of generating the HERITAGE-raster based on the building polygon layer from 3DBAG (Peters et al., 2022) and CGLC-MODIS-LCZ (Demuzere et al., 2023a) for a sample neighbourhood in southeastern Amsterdam. White background represents areas or pixels without buildings or vegetation. Pixel resolution is stated for each raster or pixel layer.

2.3 Implementation in the WRF model

This section outlines as an example how the HERITAGE-raster can be implemented in WRF. Other models with similar model structures might have a similar implementation workflow.

In WRF, all urban properties sourced and described in Table 2 and Table 3 need to be incorporated into the urban parameter lookup table (URBPARM_LCZ.TBL). We make a customised version of URBPARM_LCZ.TBL, where the 10 HERITAGE-classes takes the numbered positions of the LCZ-classes for all morphological and thermal parameters and urban fraction. Table C1 lists the corresponding parameter names in URBPARM_LCZ.TBL to the parameters identified before. Finally, we convert the raster tiff-file to geogrid binary files, create an "index"-file and modify dataset references instructing the model how and where to read the binary files (Appendix D). For further implementation details for WRF see Appendix E.

3 Results

In this section, we discuss the application of the HERITAGE-approach for Amsterdam (the Netherlands) and compare the resulting parameter values and raster to the default LCZ-raster and table values used in WRF. We also discuss some limitations and considerations for future applications of the approach for other locations.

3.1 HERITAGE parameter values

The determined wall and roof materials, thickness and composition (Table 2) clearly show the historical improvements in building insulation, technological advancement, and stricter building regulations in the Netherlands. Wall thickness has more than doubled from 18 cm before 1800 to >38 cm in building standards since 2015. Cavity walls started becoming the norm in the Netherlands around 1930 and marked a significant jump in

insulation values and lower thermal conductivity (Delft University of Technology, 2024; Rijksdienst voor het Cultureel Erfgoed, 2024; Vekemans, 2016). The most common building materials for walls are brick, mineral wool and concrete. Roofs have thickened by more than four times and had a substantial change in complexity of facet composition. The most common building materials for roofs are clay tiles, wood or chipboard, and mineral wool.

Table 2: Overview table of the HERITAGE-classes and their properties.

Class nr.	Example building	Building period	Adopted wall description			Adopted roof description			Thermal conductivity [J m^{-1} s^{-1} K^{-1}]		(Volumetric) Heat capacity [J m^{-3} K^{-1}]		Surface albedo		Surface emissivity		Window coverage fraction	Urban fraction
			Thickness [mm]	Material division [mm]	Composition (inside -> outside)	Thickness [mm]	Material division [mm]	Composition (inside -> outside)	Wall	Roof	Wall	Roof	Wall	Roof	Wall	Roof		
1		<1800	180		Pure brick	79	18-50-11	Wooden boards-air-clay tile	0.90	0.17	1 428 000	390 130	0.30	0.23	0.91	0.90	0.46	0.56
2		1800–1929	215		Pure brick	79	18-50-11	Wooden boards-air-clay tile	0.90	0.17	1 428 000	390 130	0.30	0.23	0.91	0.90	0.46	0.52
3		1930–1945	270	105-60-105	Brick-air-brick	79	18-50-11	Wooden boards-air-clay tile	0.46	0.17	1 110 935	390 130	0.30	0.23	0.91	0.90	0.46	0.48
4		1946–1964	270	105-60-105	Concrete-air-concrete	350	150-30-50-70-20-30	Reinforced concreet-perlite-air-woodwool cement slab-bitumen-gravel	0.40	0.20	1 637 957	1 387 064	0.23	0.15	0.81	0.92	0.46	0.48
5		1965–1974	300	100-100-100	Sandlime brick-mineral wool-brick	131	12-40-18-50-11	Chipboard-mineral wool-wooden boards-air-clay tile	0.10	0.09	1 076 402	391 459	0.30	0.23	0.91	0.90	0.46	0.48
6		1975–1991	300	100-50-40-100	Sandlime brick-mineral wool-air-concrete	141	12-50-18-50-11	Chipboard-mineral wool-wooden boards-air-clay tile	0.15	0.08	1 303 561	364 348	0.23	0.23	0.81	0.90	0.44	0.51
7		1992–2005	300	100-50-40-100	Concrete-mineral wool-air-brick	191	12-100-18-50-11	Chipboard-mineral wool-wooden boards-air-clay tile	0.16	0.06	1 077 694	271 377	0.30	0.23	0.91	0.90	0.48	0.52
8		2006–2014	340	100-100-40-100	Concrete-mineral wool-air-concrete	211	12-120-18-50-11	Chipboard-mineral wool-wooden boards-air-clay tile	0.10	0.06	1 060 318	246 527	0.23	0.23	0.81	0.90	0.48	0.51
9		≥2015	380	100-140-40-100	Concrete-mineral wool-air-concrete	331	12-240-18-50-11	Chipboard-mineral wool-wooden boards-air-clay tile	0.09	0.05	948 706	160 487	0.23	0.23	0.81	0.90	0.48	0.37
10		Unknown (1005)	284			177			0.36	0.12	1 230 175	443 517	0.27	0.22	0.86	0.90	0.46	0.56

We find that over the entire period the thermal conductivity decreased by 90 % and 72 % for walls and roofs, respectively (Table 2). Wall thermal conductivity decreased rapidly from 1800–1929 (HC2) until 1965–1974 (HC5) and remained fairly stable at ~13 %. Roof thermal conductivity shows a constant decline over time only interrupted by a 17 % increase for post-war buildings in 1946–1964 (HC4).

The heat capacity of both facets has also seen a general decline across time. However, the post-war housing of 1946–1964 (HC4) shows a deviation from this trend. This period marks a distinct difference in dominating building technique and materials used. Building regulations were more lenient in many countries after the second world war to accelerate the rebuilding process of the countries resulting in generally lower quality housing and worse thermal properties (Van de Voorde et al., 2015; Vekemans, 2016). In the Netherlands, this led to construction of larger buildings and more multi-unit housing out of cheaper building materials (Havinga et al.,

2020; Rijksdienst voor Ondernemend Nederland, 2022). This is reflected for HC4 in higher roof thermal conductivity and higher heat capacity of both facets.

Albedo and emissivity values are determined by the outermost material of each facet. For walls, these parameters are dictated by the use of brick or concrete, whereas roofs have prescribed clay tiles, except for HC4 which has a gravel roof. Overall, both parameters differ maximum with about 10 percent points between the HCs.

Our analysis indicates that building size does not vary that much between classes. Most HCs show fairly small buildings with mean building width varying between 12.0 m to 17.3 m and a collective mean of 13.2 m. The only exception is HC10 which has a mean of 5.8 m which could be due to it containing buildings of unknown origin which may encompass a lot of smaller buildings and structures, such as sheds and annexes which might not have required a building permit and thus a full registration.

Building height distributions follow a fairly normal distribution for most HCs with a mean building height around 12 m (Table B1). However, HC9 and HC10 show a clear right-skewed distribution which might again reflect a larger number of sheds, garages, houseboats or smaller temporary housing units. The standard deviation of the building heights has also grown over time starting at a standard deviation of 3.0 m for HC1 and ending at 8.2 m and 7.7 m for HC8 and HC9, respectively.

Table 3: Overview of morphological parameters for each HERITAGE-class for Amsterdam. If a building has a building height of <5 m it will be allocated to the "0 m" bin, and the "5 m" bin represents buildings between 5 and <10 m.

Class nr.	Building period	Building heights [m]			Building height distribution [%]						Median roof width [m]	Road width [m]
		Mean	Median	SD	< 5 m	5–10 m	10–15 m	15–20 m	20–25 m	≥ 25 m		
1	< 1800	13	13	3	2	20	64	13	1		14.4	9.4
2	1800–1929	13.3	14.3	4.2	8	14	44	33	1		12.4	15.5
3	1930–1945	12.5	13	4.1	9	17	60	13	1		12.0	17.7
4	1946–1964	11.9	11.6	5.7	11	32	39	13	5		17.3	10.5
5	1965–1974	14.3	14.1	4.9	6	14	47	24	9		16.1	12.6
6	1975–1991	12.2	12.8	4.2	11	16	61	11	1		12.8	11.5
7	1992–2005	12.7	13.2	5.2	13	16	47	20	4		12.9	9.6
8	2006–2014	13.7	13.1	8.2	13	23	39	11	5	9	15.6	8.6
9	≥ 2015	10.6	9.3	7.7	39	17	22	12	6	4	12.4	7.7
10	Unknown (1005)	7.2	4.8	4.7	59	17	16	8			5.8	11.9

Road width sees a peak in HC3 (1930–1945) at 17.7 m. Since then, the road width has decreased to its narrowest with 7.7 m for HC9 (≥2015). This could be due to a larger focus away from car-centric planning to densification and space efficiency of modern spatial planning.

Urban fractions are varying across the classes with a mean of 0.5. The highest urban fraction appears in the classes located in the inner-city area (HC1 and HC10) with a mean of 0.56. Lower densities occur in HC3–5 (1930–1974) which coincides with the tendency to build more community housing following the world wars. The newest areas

represented with HC9 (≥2015) have the lowest urban fraction which might reflect areas still in development and the city's expansion into more rural areas.

3.2 HERITAGE VS LCZ

3.2.1 Spatial class changes

The HERITAGE-raster clearly shows the historical expansion of the city (Figure 3). HC1 is clearly confined to the inner city inside a ring (the famous canal district) of what used to be the old city walls. Outside of this ring HC2 and HC3 create two layers of expansion which coincides with the growth of the population of Amsterdam beyond the city walls in the 19th century and their gradual decay and removal (Glaudemans, 2008; Tussenbroek, 2019). Newer urban expansions have been concentrated along public transport routes and major roads. Patches of one HERITAGE-class inside another dominating class also show trends of densification, and in some cases, rebuilding.

This historical expansion is less clear in the LCZ-raster since LCZs primarily focus on building morphology and density (Figure 4). Building morphology does have some relation to building period but it is often heavily dictated by the availability of land. This trend is reflected in Figure 4 where compact mid-rise (LCZ 2) dominate in the inner-city area whereas open LCZ-classes (LCZ 4–6) dominate in outer districts which also overlap with the post-war expansion of the city (see HC4–9 in Figure 3). To the northwest and southwest of the inner-city there are larger areas identified as LCZ 8 and 10 showcasing a known issue of the classification algorithms to struggle separating these two categories (Bechtel et al., 2019; Zhu et al., 2022).

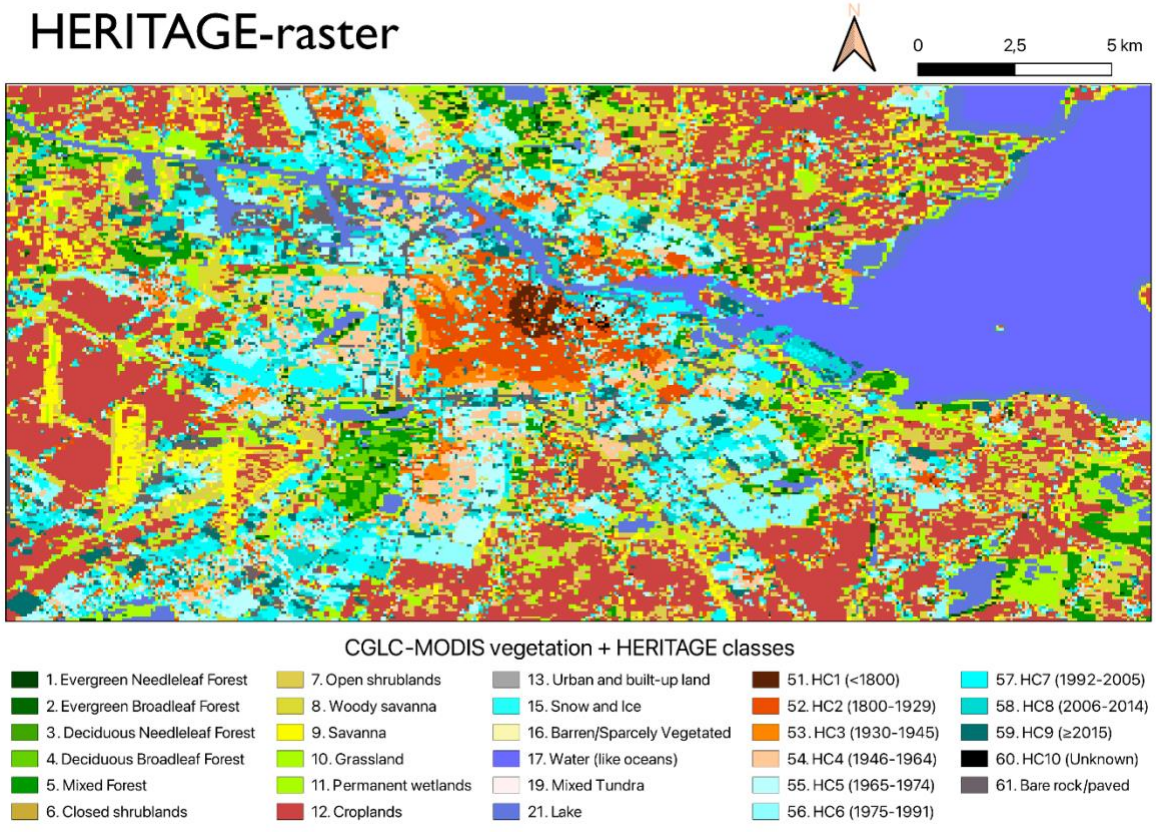


Figure 3: The HERITAGE-raster for Amsterdam with classes. Classes 1-21 and 61 are the same as for CGLC-MODIS-LCZ (Figure 4). The HERITAGE-classes (HCs) are numbered 51-60 in correspondence with their position in WRF.

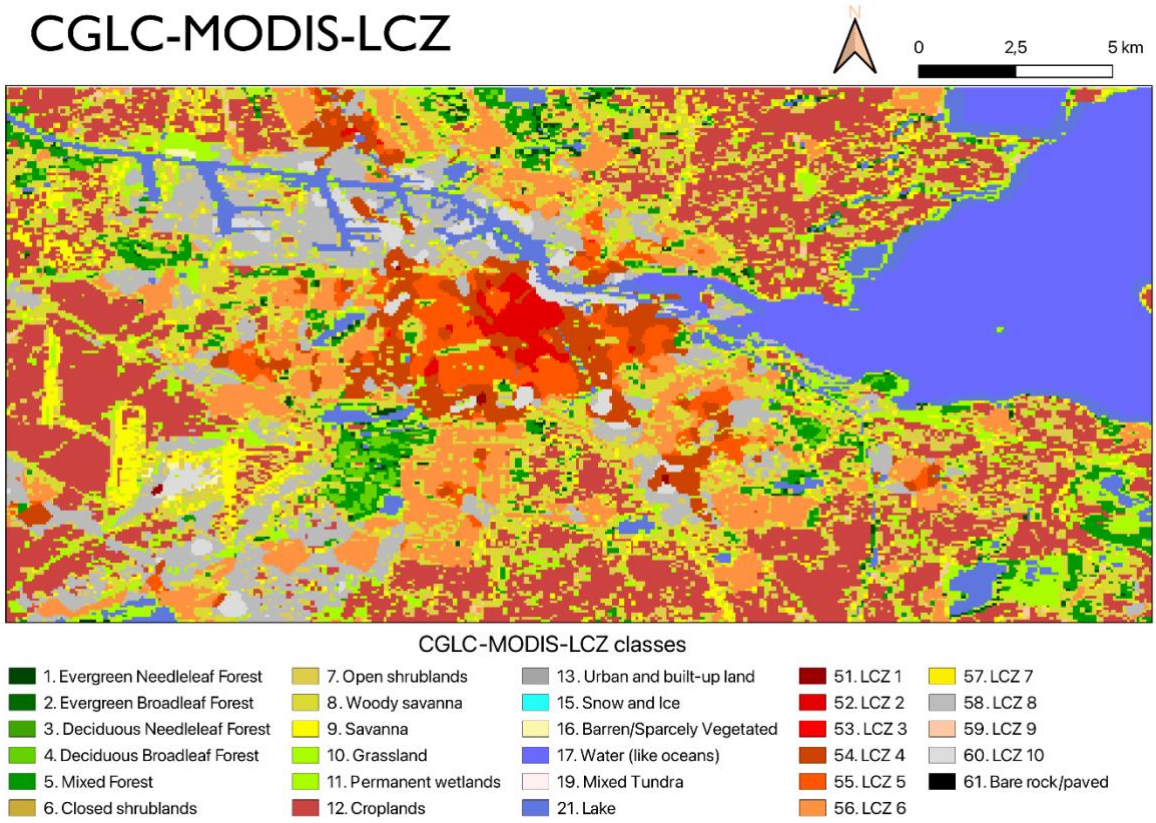


Figure 4: The CGLC-MODIS-LCZ raster for Amsterdam incorporated as the default land use map in WRF (Adapted from Demuzere et al., 2023a).

A number of differences between the default LCZ-raster and the HERITAGE-raster stands out for Amsterdam. First, the CGLC-MODIS-LCZ raster (LCZ-raster) is representative of the year 2018 (Demuzere et al., 2023b) whereas the HERITAGE-raster inherits the same vegetation layer from the LCZ-raster but is updated with urban classes based on data from 2024. This creates a difference in coverage between urban and natural vegetation classes. The HERITAGE-raster contains ~10 % more urban land cover than the LCZ-raster with 36.2 % against 26.0 %. This reduction mostly originates from a reduction in class number 8 (woody savanna) with 4.2 % (Table 4). The difference in representation year also causes the LCZ-raster to miss recent urban developments, for example at the eastern harbour.

Each HC replaces multiple LCZ-classes revealing no clear connection between the two classification schemes (Figure 5). The non-compact low-rise classes (LCZs 6 and 8) are the most frequently occurring LCZs and are spatially overlapping with 9 out of 10 HCs. Only HC1 (<1800) sees a majority of its buildings belonging to one class, LCZ 2. HC6 (1975–1991) and HC7 (1992–2005) are the most frequent HCs in Amsterdam representing 38.7 % of the building pixels in the HERITAGE-raster. HC5 and HC6 have a similar distribution of LCZs probably reflecting a similar development policy in this period (1965–1991). All HCs show a displacement of vegetation of 11–43 % compared to the LCZ-raster, but this is partially offset by the increase in vegetation fraction within each HC.

Table 4: Occurrence of the different classes in the HERITAGE-raster compared to the default CGCL-MODIS-LCZ raster. Note that classes nr. 51-60 represent the HERITAGE-classes and the LCZ-classes for the HERITAGE- and the LCZ-raster, respectively and cannot be directly compared.

Class nr.	HERITAGE-raster class name	LCZ-raster class name	HERITAGE coverage [%]	LCZ-raster coverage [%]
1	Evergreen Needleleaf Forest		0.51	0.59
4	Deciduous Broadleaf Forest		0.47	0.48
5	Mixed Forest		3.25	3.63
7	Open shrublands		5.34	6.43
8	Woody savanna		8.34	12.62
9	Savanna		3.68	4.31
10	Grassland		1.90	2.57
11	Permanent wetlands		3.15	3.95
12	Croplands		19.58	21.14
16	Barren/sparsely vegetated		0.07	0.08
17	Water (like oceans)		12.43	12.74
21	Lake		5.09	5.42
51	HC1 (<1800)	LCZ 1 (Compact high-rise)	0.35	0.04
52	HC2 (1800-1929)	LCZ 2 (Compact mid-rise)	4.23	0.74
53	HC3 (1930-1945)	LCZ 3 (Compact low-rise)	1.71	0.02
54	HC4 (1946-1964)	LCZ 4 (Open high-rise)	3.88	3.95
55	HC5 (1965-1974)	LCZ 5 (Open mid-rise)	3.82	2.83
56	HC6 (1975-1991)	LCZ 6 (Open low-rise)	6.85	8.56
57	HC7 (1992-2005)	LCZ 7 (Lightweight low-rise)	5.81	-
58	HC8 (1992-2014)	LCZ 8 (Large low-rise)	3.57	8.24
59	HC9 (≥2015)	LCZ 9 (Sparsely built)	2.70	0.23
60	HC10 (Unknown)	LCZ 10 (Heavy industry)	0.02	1.44
61	Bare rock/paved		3.25	-

As expected, ~64 % of the raster pixels stay the same and at least 65 % of the spatial occurrence is preserved between the rasters for all vegetation classes (Figure F1). Among the urban classes, the most common replacement is for the compact LCZ-classes. 59 % of LCZ 3 (compact low-rise) tiles are replaced with HC2 (1800–1929), while LCZ 2 (compact mid-rise) is replaced with HC2 and HC1 (<1929) in about 52 % and 27 % of the cases, respectively. LCZ 1 is rarely occurring in Amsterdam but is usually replaced with HC7 or HC8 (1992-2014). Open low-rise buildings (LCZ 6) are in 24 % of the cases replaced with HC6 (1975–1991), while large low-rise buildings (LCZ 8) are in 40 % of the cases replaced with HC7 (1992–2005) or reclassified to a sealed surface type. It is also interesting to note that LCZ 1 is only appearing since HC5 (≥1965), and the growing dominance of more recent HCs are both evidence of the growing building stock and tendency to build higher and denser.

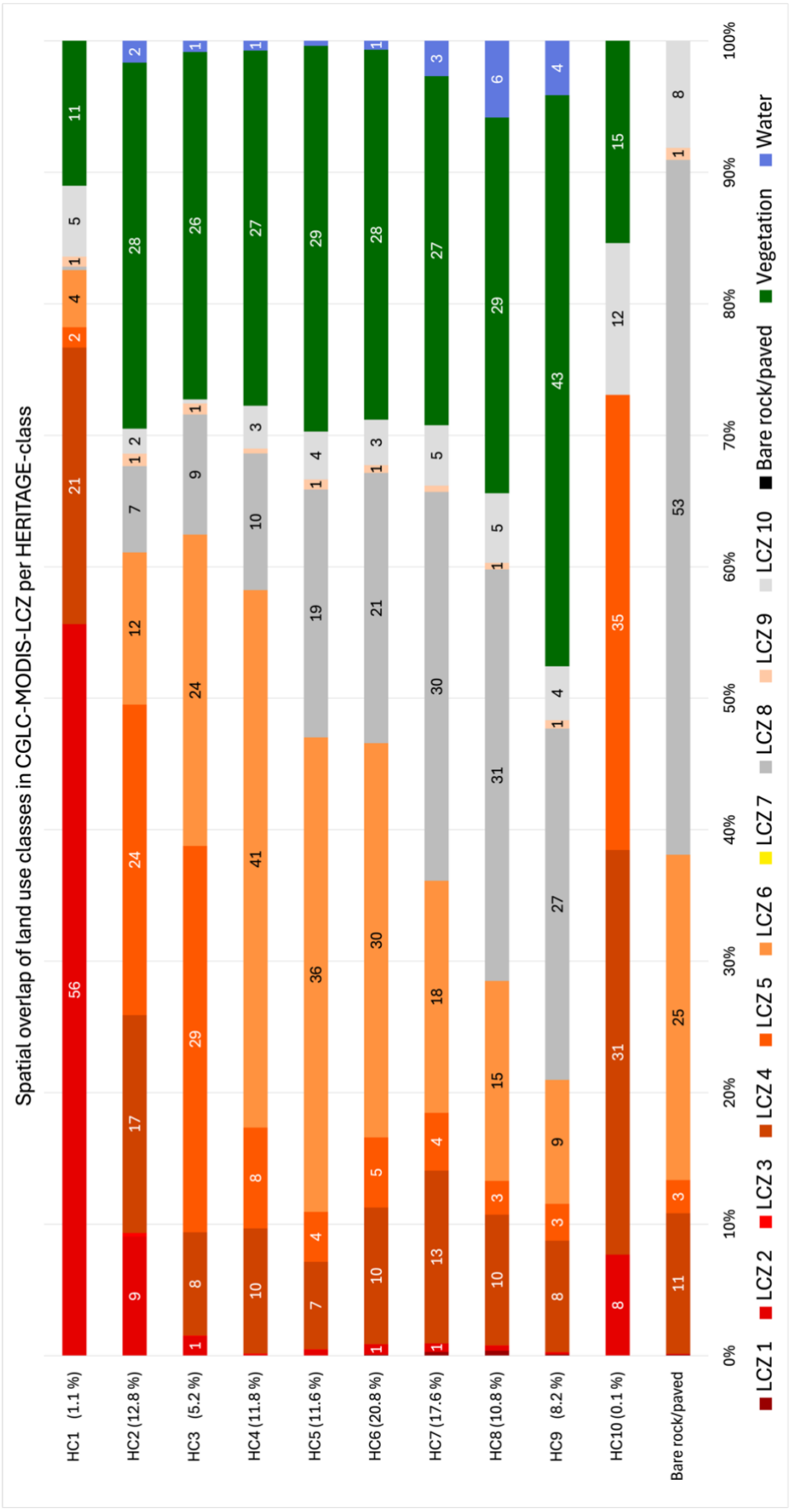


Figure 5: Spatial overlap between the HERITAGE-classes and the land use classes in CGLC-MODIS-LCZ. Percentages behind the HCs refer to their relative occurrence of all building classes in the HERITAGE-raster.

3.2.2 Comparison of parameter values in WRF

We find considerable numerical differences between the default LCZ parameter values and the HERITAGE-classes for Amsterdam. Table B1 shows the tabular values for the two classes. The values for the LCZs are taken from the default URBPARM_LCZ.TBL in WRF whereas the HERITAGE values are the same as in Table 2 andTable 3.

A large difference appears between the two classification systems for the building morphological parameters. Mean building height across all classes are higher for the LCZs mainly driven by the high-rise classes (LCZ 1 and 4). The building height distributions are also very different. The high-rise-classes show a clear shift in distribution to the right compared to the other LCZs with a mean of 37.5 m for SLUCM and 50 m for BEP(+BEM). Except for the high-rise classes and LCZ 10, none of the other LCZs follow a normal distribution of building height and most have a right skewed distribution. Building heights are more similar for the HCs with a collective mean of about 12 m and building height distributions closer to a normal distribution for all classes except HC9 and HC10 which show lower means and right skewed distributions. Standard deviations for building heights are considerably higher and more variable for the HCs than for the LCZs where only LCZs 1 and 2 have a standard deviation higher than 1 m. The mean standard deviation for the HCs is almost 3.5x the mean standard deviation for the LCZs which is an effect of incorporating different building types inside each HC. LCZ buildings and roads are also on average around twice as wide as the HCs.

Urban fraction shows a large variation for the LCZs ranging from 30 % to 95 %. The HCs show lower values and more stability in urban fraction with values between 37 % and 56 %. Excluding both LCZ 1 and 9 – representing together <1 % of the tiles and the extreme ends of the urban fraction distribution – the urban fraction spread is 35 % [55–90 %] for LCZs which is still greater than the 24 % spread for the HCs. The LCZs have a mean urban fraction of 72 % whereas the HCs have a mean of 50 %. This shows that there is a slight compensation in the HERITAGE-raster related to the amount of vegetation; there is a lower amount of vegetation tiles (~10 % less) but a larger green fraction (~50 %) in the urban HERITAGE tiles compared to the LCZs.

One of the main differences and strengths that the HERITAGE-approach offers is the diversity in thermal properties per class based on historical and spatial data. It is clear from Table B1 that all LCZs are represented identical from a thermal perspective. The mean heat capacity for the HCs is for roofs 66 % lower and for walls 20 % lower than the corresponding LCZ value. Mean thermal conductivity is 92 % lower for roofs and 76 % lower for walls in the HERITAGE-approach. For the HCs, mean roof heat capacity is 444 kJ m^{-3} K^{-1} with a value range of 1 227 kJ m^{-3} K^{-1}. Wall heat capacity has a mean of 1 230 kJ m^{-3} K^{-1} and a value range of 689 kJ m^{-3} K^{-1}. The mean albedo estimates with range are 0.22 [0.15–0.23] for roofs and 0.27 [0.23–0.30] for walls. Values of mean emissivity with its range are 0.90 [0.90–0.92] for roofs and 0.86 [0.81–0.91] for walls. The relatively small value range for albedo and emissivity reflects the strong tradition of using clay tiles for roofing, and bricks for walls in construction work in the Netherlands.

On average, the HCs show lower values for all thermal properties than the LCZs. The largest differences between the two approaches show up for heat capacity and thermal conductivity. This is where the assumptions of the facet

compositions matter the most since all of them influence the final value entering the model. Compared to the LCZ values, only HC4 has a higher heat capacity for both facets. This indicates that on average LCZs assume a higher storage capacity for heat than is present according to the literature review. LCZs also assume a higher thermal conductivity for all buildings than the literature review suggest. This means that heat is transferred quicker through the facets and the building envelope can accumulate more heat using the LCZ approach. Most of the HCs suggest that the studied buildings transfer heat slower through the facets and the walls have a lower heat storing capacity than previous model exercises using LCZs may indicate.

4 Discussion

4.1 Comparison to other studies

To the best of our knowledge, the HERITAGE-approach is the first building classification methodology developed with the primary goal of improving the representation and understanding of the impact of historical construction on meteorological variables for urban numerical modelling. Building classification based on (historical) construction archetypes is a common exercise in energy building modelling research (Carnieletto et al., 2021), but is absent from most meteorological and climate research.

Aksoezen et al. (2015) found a statistical relationships between building age, energy demand and compactness (surface area to volume ratio) which relates to anthropogenic heat emissions and morphological aspects which affect the microclimate. Pappaccogli et al. (2021) used three building classes in their WRF simulations but thermal properties only varied with building function (residential VS industrial/commercial use). T17 expanded building classes developed for energy consumption analysis in the TABULA-project (TABULA Project Team, 2012), and is the only study assessing the change of the energy balance for multiple construction periods.

Compared to the model studies by T17 and Pappaccogli et al. (2021), the HERITAGE-approach creates more detailed and longer historical representation of building classes. The former study groups buildings mainly based on French thermal regulations resulting in all buildings constructed before 1949 to belong to the same class. In comparison, we identify three HERITAGE-classes before 1946 for Amsterdam, also considering historical documents on construction practices before thermal regulations were implemented. For TEB modelling purposes T17's classes are sorted based on three steps: 1) morphology, 2) thermal properties, and 3) use function. This results in a potentially more accurate building classification but is also considerably more data intensive than our approach. T17 also mention uncertainties in how to categorise buildings with uncertain or mixed use. The HCs do not assume any particular building use, but depending on the urban model it is possible to prescribe different heating/cooling regimes to reflect different energy use.

In our spatial comparison analysis of HCs to LCZs we find multiple LCZs occurring within each HCs. This aligns with recent findings of Habib et al. (2026) where they used a clustering approach to categorise Dutch neighbourhoods into (sub-)LCZ classes based on morphological and vegetation data. They found the frequency distribution of four architectural building periods to vary across their seven identified clusters. Their algorithm also classifies most of the central area of Amsterdam – overlapping with large parts of HC1–3 in Figure 3 and

LCZ 2, 4 and 5 in Figure 4 – as LCZ 2 with mean building heights of 9–17 m. This finding aligns well with the building heights for HC1–3 (Table 3) but also illustrates how sensitive LCZ mapping approaches are to mapping subjectivity.

Our study introduces the new perspective of categorising building classes based on a "thermal property centric" view while utilising existing numerical modelling infrastructure. This enables urban numerical modelling where thermal and morphological properties are disentangled, providing flexibility of integration into different models at various scales (LES and meso) and uses (e.g. microclimate or building energy modelling). The tables presented provide a detailed foundation that makes it easier to implement building properties for urban models with different requirements on level of detail. These parameter values provide a generalised first order estimate of thermal properties when detailed information on building level is lacking. This would also make it interesting to use as a possible starting point for building energy modelling purposes.

The HCs presented here provide customised thermal and morphological values for Amsterdam, but the methodology described above can be applied to other locations with similar data sources available. Given the domination of brick-based construction in the Netherlands, other Dutch cities can reasonably assume the same thermal property values (Table 2) but should consider recalculating the morphological statistics (Table 3) and urban fraction using 3DBAG and local cadastre data if the city is considerably differently structured. Applying the HERITAGE-approach to a non-Dutch setting requires – besides the local building construction literature review – shapefiles of roads and buildings (including building height and building year) and a spatial dataset of vegetation fraction.

4.2 Limitations and uncertainty

Urban environments vary greatly between countries, regions and even within city districts depending on historical developments and local practices. This fact makes every attempt at generalisation through categorisation to have limits in application. In this paper, we have outlined an approach for how to categorise buildings based on their thermal properties identified from literature on different historical construction practices in Amsterdam. The values from all tables are therefore only a good representation of Amsterdam. We would only consider regions with a similar historical building practice and morphological structure to be able to reasonably apply the same values. However, we consider the *thermal* properties to be representative for most cities in the Netherlands and potentially parts of Belgium and Germany, but a local expert assessment should be conducted before making this assumption. Morphological values and urban fractions need to be collected for the region of interest following an approach similar to what we describe in Sect. 2.

The urban modelling community is generally aware that the default values for the LCZs are not representative for many urban environments, especially at finer scales (Hammerberg et al., 2018; Huang et al., 2023; Stewart and Oke, 2012; Zonato et al., 2020). WRF was developed by NCAR and the current default urban variables are based on global averages from Stewart and Oke (2012) (Cenlin He, 2024). Most urban modelling studies use these values for their cities despite the following warning in the urban parameter tables in WRF: "The default [parameter] values are probably not appropriate for any given city. Users should adapt these values based on the

city they are working with." This calls for the same customised approach for the urban morphology parameters as mentioned for the HERITAGE-approach.

When developing the HERITAGE-approach, we found that the estimation of urban fractions is highly sensitive to the input data used, especially based on resolution. We compared the urban fraction values per HERITAGE-class based on data from Ronda et al. (2017) to values obtained using the global urban fraction dataset by Patel and Roth (2022). The data from Ronda et al. (2017) was calculated based on NDVI data from 2008 and has a resolution of ~ 30 m, whereas the data from Patel and Roth (2022) was based on land cover data from 2021 with a ~100 m resolution. The mean and range of the urban fraction based on the former dataset was 50 % [37–56 %], compared to 59 % [54–74 %] for the later. Despite the older age, we opted for the higher resolution dataset as it demonstrated the sharp contrast and heterogeneity present in Amsterdam better.

Cutoffs between HCs were selected based on building years obtained from the literature (Table A1). The parameters of the resulting 10 classes were prepared to align with WRFs current code infrastructure and with urban modelling applications in mind. More or fewer classes might be relevant for other urban areas. The HCs outlined in this paper serve as an example and should be updated in the future as the city develops and more data becomes available.

Assumptions about facet composition and parameter values were made due to a lack of data for many parameters in the Netherlands. Because the Netherlands lacks a centralised database for construction practice, we had to derive materials and facet compositions from literature to estimate all thermal parameter values. Moreover, some buildings might have undergone refurbishments (e.g. post-insulation) since they were built. This leads to these houses having a different "thermal footprint" compared to what the literature suggest. Unfortunately, there is no central registry for refurbishments in the Netherlands. Therefore, representative parameter values were assumed based on the literature and mean parameter values for different materials from lookup tables. Among these parameters, albedo and emissivity are parameters which may vary greatly depending on the facet surface regardless of building period. Future efforts should therefore concentrate on establishing a database for these parameters, ideally on building level, to reduce uncertainty in these estimates. In its current form the HCs represent a conservative non-retrofit building state.

5 Conclusion

Urban climate modelling is crucial for planning and understanding the impact of weather on energy demand, urban heat and health. The accuracy of the urban representation in these models can significantly alter the modelling results and thus society's preparedness under extreme conditions. Past urban modelling efforts have overwhelmingly focused on the characterisation and mapping of the morphological parameters of cites but ignored the potential impact of thermal properties of the buildings themselves.

This study demonstrates a new and alternative classification and modelling approach for urban numerical weather and climate modelling based on historical construction practices and thermal properties, i.e. the HERITAGE-

approach. The conventional approach of categorising buildings and neighbourhoods using LCZs are subject to significant mapping subjectivity and simplification of the morphology which may reduce a model's ability to capture the urban heterogeneity. Compared to the conventional LCZ approach, the HERITAGE-approach offers a novel method for developing literature- and data-based urban classes with customised spatially varying morphological and thermal parameter values which are more representative of the real world.

We apply our new approach on Amsterdam (the Netherlands) and compare the result with the default LCZ values and LCZ-raster in WRF. We identify 10 HERITAGE-classes (HCs) based on different building periods and estimate their respective thermal and morphological properties as well as their location. The HERITAGE-raster exhibits an updated land use map with urban developments not captured in the LCZ-raster. Little spatial correlation is found between specific LCZs and HCs.

For Amsterdam, the HCs show generally smaller variability in morphology parameters between classes, but larger building height variability within a class compared to the LCZs. The difference between LCZ and HERITAGE values for albedo and emissivity is on average only 8 % and 3 % lower respectively for the HCs due to the extensive use of bricks in the Netherlands. All HCs show higher thermal conductivity and 9 out of 10 classes show higher heat capacity for both walls and roofs compared to standard LCZ values in WRF. Compared to previous model exercises using LCZs, the HERITAGE-approach suggest that the buildings studied transfer heat slower through the facets and the heat storing capacity of the walls are lower. The effect of this building representation in modelling will be explored in a follow up paper.

The HCs contain all variables required – except anthropogenic heat related parameters – for conducting thermal and energy assessments, and modelling of the urban environment using numerical models such as WRF. Being a "thermal property centric" classification, the HERITAGE-approach allows for disentangling thermal and morphological parameter values making it suitable for modelling applications at different scales. This new approach has the potential to give researchers and policy makers new insights into the origin and spatial variability of urban meteorological variables, such as temperature, and learn from past construction practices to improve urban living conditions and future construction practices.

Appendix A: Sources

Table A1: Overview of the sources used in the literature review with their respective use.

Used for	Source
Roof construction and material	(Oltengarm et al., 2001)
Rc values and insulation	(Kuijeren, 2024)
Rc values and insulation	(Keesjan, 2020)
Insulation	(Foil insulation: to gap or not to gap? That is the question!: Do I need an air gap when using foil insulation: Do I need an air gap when using foil insulation, 2024)
Window coverage fraction	(Dang et al., 2024)
Rc values and insulation	(Isolatiewaarde: de Rd waarde, Rc waarde en lambdawaarde, 2024)
Example housing in the Netherlands	(Rijksdienst voor Ondernemend Nederland, 2022)
Post-war buildings	(Van de Voorde et al., 2015)
Cavity walls	(Rijksdienst voor het Cultureel Erfgoed, 2024)
Amsterdam building history	(Tussenbroek, 2019)
History of Dutch brickwork and building codes	(Vekemans, 2016)
Rc values and insulation	(Kim, 2022)
Building regulations	(van Overveld et al., 2011)
Historical buildings in Amsterdam	(Glaudemans, 2008)
Insulation	(Scottish Government, 2020)
Cavity walls	(Rob, 2023)
Dutch brick history	(Orsel, 2006)
Roof construction and materials	(Oltengarm et al., 2001)
Historical building construction	(Museum Ons' Lieve Heer op Solder, 2024)
Roof insulation	(Milieu Centraal, 2024)
Rc values and building regulations	(Liebregts and Persoon, 2011)
Building construction	(Koninklijk Verbond van Nederlandse Baksteenfabrikanten, 2002)
Cavity walls	(Koninklijk Verbond van Nederlandse Baksteenfabrikanten, 1999)
Cavity wall construction	(Historic England, 2012)
Heritage value, post-war buildings	(Havinga et al., 2020)
Dutch building stock composition	(Delft University of Technology, 2024)
U-values and thermal conductivity	(Building Research Establishment, 1984)

582 **Table A2: Overview table of building materials and their estimated thermal property values based on the literature**
583 **search with the associated sources.**

Facet	Material	Average thermal conductivity [W $m^{-1} K^{-1}$]	Average specific heat capacity [J $kg^{-1} K^{-1}$]	Surface albedo	Surface emissivity	Source
Both	Air	0.02	1005			(Building Research Establishment, 1984; Table 15 Thermal Resistances of Air Gaps, 2021)
	Mineral wool	0.038	920			(Table 6 Thermal Conductivity, Specific Heat Capacity and Density, 2024; The Engineering Toolbox, 2003b; Koninklijk Verbond van Nederlandse Baksteenfabrikanten, 2002)
Wall	Brick	0.9	840	0.3	0.91	(Koninklijk Verbond van Nederlandse Baksteenfabrikanten, 2002; Oke, 1987; Rasooli, 2020; The Engineering Toolbox, 2003a)
	Concrete	0.68	940	0.225	0.805	(Table 6 Thermal Conductivity, Specific Heat Capacity and Density, 2024; The Engineering Toolbox, 2003a; Koninklijk Verbond van Nederlandse Baksteenfabrikanten, 2002; Oke, 1987)
	Sand lime brick	0.64	1000			(Jasińska et al., 2021; de Vree, 2026)
Roof	Wooden boards	0.14	1200			(Table 6 Thermal Conductivity, Specific Heat Capacity and Density, 2021)
	Clay tile	0.8	800	0.225	0.9	(Table 6 Thermal Conductivity, Specific Heat Capacity and Density, 2024; The Engineering Toolbox, 2003a; Oke, 1987)
	Reinforced concrete	1.442	1000			(Farhan et al., 2021)
	Woodwool cement slab	0.085	1000			(Building Research Establishment, 1984; Table 6 Thermal Conductivity, Specific Heat Capacity and Density, 2021)
	Bitumen	0.5	1000			(Table 6 Thermal Conductivity, Specific Heat Capacity and Density, 2021)
	Gravel	0.36	840	0.15	0.92	(Oke, 1987; Oke et al., 2017; Pisello et al., 2014)
	Chipboard	0.15	2093			(Table 6 Thermal Conductivity, Specific Heat Capacity and Density, 2021)
	Perlite	0.08	837			(Table 6 Thermal Conductivity, Specific Heat Capacity and Density, 2021)

584

Appendix B: HERITAGE VS LCZ values in WRF

Table B1: Variable values for urban classes in WRF. The left table shows default values for the LCZs and the right table shows customised HERITAGE-class values for Amsterdam. Mini histograms to the right visualise the building height distribution for BEP(+BEM).

LCZ-class	SLUCM										BEP / BEP+BEM												
	Building height [m]	SD building height [m]	Roof width [m]	Road width [m]	Urban fraction	Roof heat capacity [J m^{-3} K^{-1}]	Wall heat capacity [J m^{-3} K^{-1}]	Roof thermal conductivity [J m^{-1} s^{-1} K^{-1}]	Wall thermal conductivity [J m^{-1} s^{-1} K^{-1}]	Roof albedo	Wall albedo	Roof emissivity	Wall emissivity	Building heights distribution [%]									
														5 m	10 m	15 m	20 m	25 m	30 m	35 m	40 m	45 m	50 m	55 m	60 m
1	37.5	4.0	22.2	20.0	0.95	1 320 000	1 540 000	1.54	1.51	0.30	0.30	0.90	0.90												
2	17.5	3.0	22.0	14.0	0.90	1 320 000	1 540 000	1.54	1.51	0.30	0.30	0.90	0.90				50	50							
3	6.5	1.0	9.6	5.2	0.85	1 320 000	1 540 000	1.54	1.51	0.30	0.30	0.90	0.90	72	28										
4	37.5	1.0	42.9	50.0	0.65	1 320 000	1 540 000	1.54	1.51	0.30	0.30	0.90	0.90								17	21	24	21	17
5	17.5	1.0	26.3	35.0	0.70	1 320 000	1 540 000	1.54	1.51	0.30	0.30	0.90	0.90			50	50								
6	6.5	1.0	13.0	13.0	0.60	1 320 000	1 540 000	1.54	1.51	0.30	0.30	0.90	0.90	72	28										
7	3.0	1.0	25.0	3.3	0.85	1 320 000	1 540 000	1.54	1.51	0.30	0.30	0.90	0.90	100											
8	6.5	1.0	28.9	32.5	0.85	1 320 000	1 540 000	1.54	1.51	0.30	0.30	0.90	0.90	72	28										
9	6.5	1.0	43.3	43.3	0.30	1 320 000	1 540 000	1.54	1.51	0.30	0.30	0.90	0.90	72	28										
10	10.0	1.0	23.8	28.6	0.55	1 320 000	1 540 000	1.54	1.51	0.30	0.30	0.90	0.90	16	68	16									
LCZ mean:	14.9	1.5	25.7	24.5	0.72	1 320 000	1 540 000	1.54	1.51	0.30	0.30	0.90	0.90	36.7	16.4	10.5	9.1	0.0	0.0	0.0	3.1	3.8	4.4	3.8	3.1

HERITAGE-class	SLUCM										BEP / BEP+BEM												
	Building height [m]	SD building height [m]	Roof width [m]	Road width [m]	Urban fraction	Roof heat capacity [J m^{-3} K^{-1}]	Wall heat capacity [J m^{-3} K^{-1}]	Roof thermal conductivity [J m^{-1} s^{-1} K^{-1}]	Wall thermal conductivity [J m^{-1} s^{-1} K^{-1}]	Roof albedo	Wall albedo	Roof emissivity	Wall emissivity	Building heights distribution [%]									
														5 m	10 m	15 m	20 m	25 m	30 m	35 m	40 m	45 m	50 m	55 m	60 m
1	13.0	3.0	14.4	9.4	0.56	390 130	1 428 000	0.17	0.90	0.23	0.30	0.90	0.91	2	20	64	13	1							
2	13.3	4.2	12.4	15.5	0.52	390 130	1 428 000	0.17	0.90	0.23	0.30	0.90	0.91	8	14	44	33	1							
3	12.5	4.1	12.0	17.7	0.48	390 130	1 110 935	0.17	0.46	0.23	0.30	0.90	0.91	9	17	60	13	1							
4	11.9	5.7	17.3	10.5	0.48	1 387 064	1 637 957	0.20	0.40	0.15	0.23	0.92	0.81	11	32	39	13	5							
5	14.3	4.9	16.1	12.6	0.48	391 459	1 076 402	0.09	0.10	0.23	0.30	0.90	0.91	6	14	47	24	9							
6	12.2	4.2	12.8	11.5	0.51	364 348	1 303 561	0.08	0.15	0.23	0.23	0.90	0.81	11	16	61	11	1							
7	12.7	5.2	12.9	9.6	0.52	271 377	1 077 694	0.06	0.16	0.23	0.30	0.90	0.91	13	16	47	20	4							
8	13.7	8.2	15.6	8.6	0.51	246 527	1 060 318	0.06	0.10	0.23	0.23	0.90	0.81	13	23	39	11	5	9						
9	10.6	7.7	12.4	7.7	0.37	160 487	948 706	0.05	0.09	0.23	0.23	0.90	0.81	39	17	22	12	6	4						
10	7.2	4.7	5.8	11.9	0.56	443 517	1 230 175	0.12	0.36	0.22	0.27	0.90	0.86	59	17	16	6	2							
HC mean:	12.1	5.2	13.2	11.5	0.50	443 517	1 230 175	0.12	0.36	0.22	0.27	0.90	0.86	17.1	18.6	43.9	15.6	3.5	1.3	0.0	0.0	0.0	0.0	0.0	0.0

Appendix C: WRF parameter names

Table C1: Corresponding parameter names in URBPARM.TBL in WRF.

Parameter name	Name in URBPARM.TBL
Building heights mean [m]	ZR
Building heights SD [m]	SIGMA_ZED
Median roof width [m]	ROOF_WIDTH
Road width [m]	ROAD_WIDTH
Urban fraction	FRC_URB
Roof (volumetric) heat capacity	CAPR
Wall (volumetric) heat capacity	CAPB
Road width [m]	STREET PARAMETERS: street width
Median roof width [m]	STREET PARAMETERS: building width

Parameter name	Name in URBPARM.TBL
Roof thermal conductivity	AKSR
Wall thermal conductivity	AKSB
Roof surface albedo	ALBR
Wall surface albedo	ALBB
Roof surface emissivity	EPSR
Wall surface emissivity	EPSB
Window coverage fraction [%]	PWIN
Building height distribution 5 m bins per class	BUILDING HEIGHTS

Appendix D: Technical details for implementing the HERITAGE-raster in WRF

The HERITAGE-raster needs to be converted to a readable binary format for WRF and appropriate changes need to be added to the preprocessing modules in WRF. We used the convert_geotiff tool (Beezley et al., 2025) to convert the raster tiff-file to geogrid binary files using the following command:

convert_geotiff -c 60 HERITAGE-raster_final.tif

This creates multiple files labelled "00XXX-00XXX.00XXX-00XXX" and an "index"-file. It is necessary to add the line: "*mminlu="MODIFIED_IGBP_MODIS_NOAH*" to the index-file. All of these files are then added to a "HERITAGE"-folder which should be placed in the same directory as the other land surface files (e.g. LCZ rasters) and needs to be pointed to in the GEOGRID.TBL and the namelist.wps.

In the GEOGRID.TBL the following lines need to be added above the existing LANDUSEF section:

```
==============================
name=LANDUSEF                    #Insert HERITAGE-raster
    priority = 3
    dest_type = categorical
    z_dim_name = land_cat
    interp_option = default:nearest_neighbor
    abs_path = default: <HERITAGE folder location>
==============================
name=LANDUSEF                    #Insert CGLC_MODIS_LCZ_global as backup
    priority = 2
    dest_type = categorical
    z_dim_name = land_cat
    interp_option = default:nearest_neighbor
```

rel_path = default:CGLC_MODIS_LCZ_global/

==========

To link the HERITAGE-raster in the WPS, the following lines need to be changed in the namelist.wps:

geog_data_res = 'default','default','default','default',

geog_data_path = '<location of land surface files and HERITAGE folder>'

opt_geogrid_tbl_path = './'

It is important to refer to and store the files correctly. The abs_path in GEOGRID.TBL needs to point to where the HERITAGE-folder with the converted binary-files and the index-file is located. The geog_data_path in namelist.wps needs to point to the directory where all land surface files are located. Note that geog_data_res is set to 'default' and is aligned with the selection for interp_option, abs_path and rel_path. This results in a smooth transition between datasets as they are available regardless of nesting domain.

Appendix F: Conversion of land use classes from CGLC-MODIS-LCZ to HERITAGE

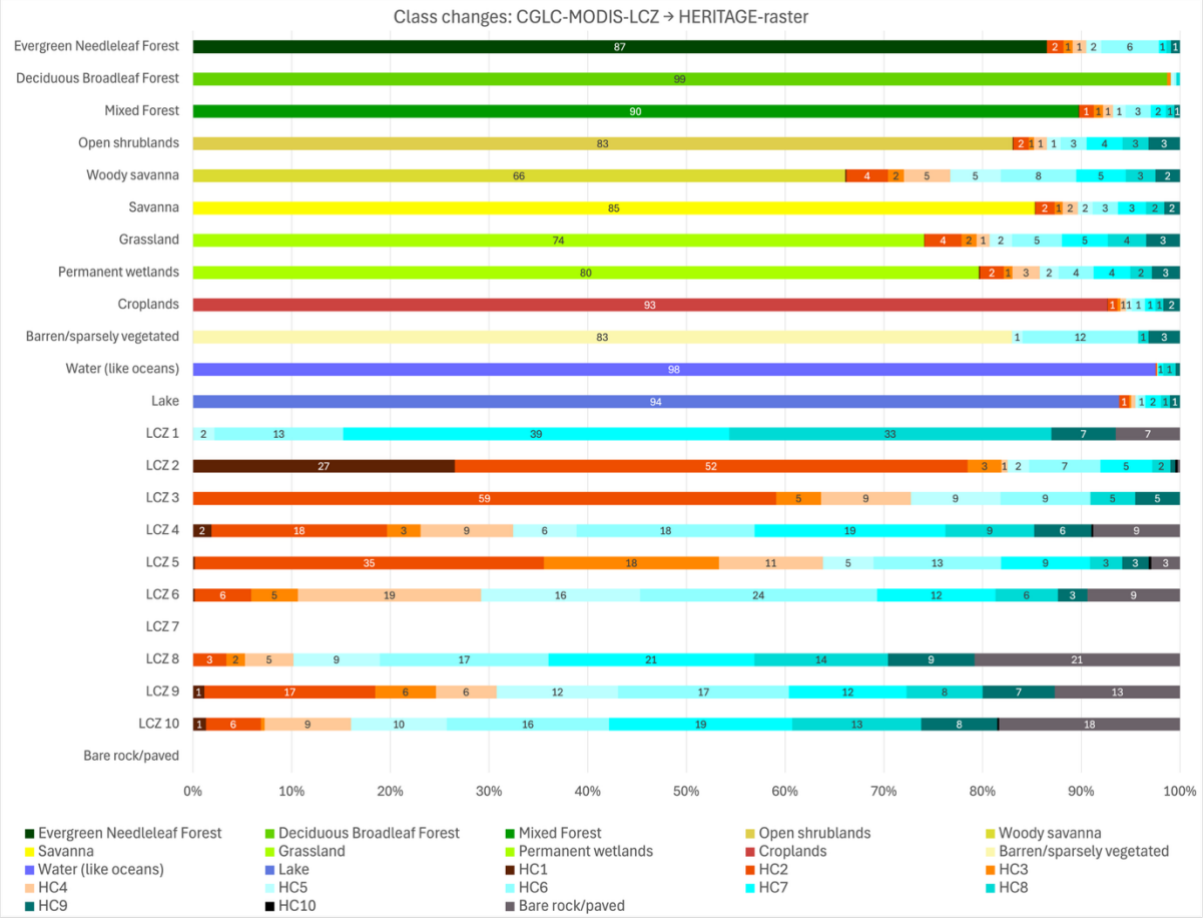


Figure F1 shows the changes of land use classes moving from the CGLC-MODIS-LCZ raster to the HERITAGE-raster. Most of the natural classes stay the same and there is not a clear link between specific LCZs and specific HCs.

Appendix E: Additional implementation details for WRF

Two additional changes are needed to make the representation fair for all HERITAGE-classes due to the facet representation in WRF. Each facet in WRF is separated into four layers with a fixed layer thickness dependent on the urban scheme (SLUCM=20 cm, BEP(-BEM)=15.75 cm). The facet thermal properties are applied across all layers (Kusaka *et al.*, 2001; Martilli, Clappier and Rotach, 2002). To account for this model aspect we suggest to calculate the equivalent thermal conductivity per facet and HERITAGE-class following (Pappaccogli *et al.*, 2018):

$$\lambda_{e,HC} = (\lambda_{HC} * L_{HC})/L_{WRF} \quad (1)$$

where λ_{HC} is the original thermal conductivity of the HERITAGE-class facet, while L_{HC} and L_{WRF} represent the facet thickness (roof or wall) of the HERITAGE-class and in WRF, respectively. Our resulting equivalent thermal conductivity is incorporated into the modified version of the URBPARM_LCZ.TBL (Sandvik, Milošević and Steeneveld, 2026). Be aware that one needs to set *use_wudapt_lcz=1* in the namelist.input to make WRF read the URBPARM_LCZ.TBL.

Upon model testing with WRF version 4.6.1 we encountered model instability for BEP and BEP-BEM due to low roof thermal conductivity values. To avoid this instability, we suggest adjusting the roof layer thickness (*dzr_u* and *dzr*) inside WRF for BEP and BEP-BEM. We obtained satisfactory results when increasing the two outermost layers from 0.5 to 1 cm and 0.25 to 4 cm for these two urban canopy schemes resulting in a total modelled roof thickness of 20 cm instead of 15.75 cm. We conducted a sensitivity test to the increase in roof thickness and found a minimal impact on our simulation results (difference <5%). An additional benefit of increasing the roof thickness to 20 cm is that the equivalent thermal conductivity for roofs stays the same regardless of urban canopy scheme.

Code and data availability

The HERITAGE approach has been tried and tested in WRFv4.6.1 but should in principle work for any version of WRF with the LCZ representation enabled (since WRFv4.3). Other models with a similar structural setup and requirements to WRF could also implement the HERITAGE approach in a similar way.

The HERITAGE-raster.tiff with corresponding binary and index-file for WRF as well as the HERITAGE-modified URBPARM_LCZ.TBL are available at 4TU.ResearchData: https://doi.org/10.4121/8687610F-A25E-49CA-ADC6-8BCCE0F5A22B (Sandvik et al., 2026). The WRF source code is openly available on GitHub (Weather Research and Forecasting Model, 2026) and our modified and tested version of WRFv4.6.1 along with the GEOGRID.TBL is available in the 4TU.ReserachData repository above. Other underlying data can be provided by the corresponding authors upon request.

Author contributions

BES performed the conceptualisation, data curation, formal analysis, investigation, software, validation, visualization and writing. GJS contributed to the conceptualisation, data curation, funding acquisition, project administration, resources, supervision, review and editing of the study. DM contributed to the conceptualisation, supervision, review and editing of the study.

Competing interests

The authors declare that they have no conflict of interest.

Acknowledgements

We acknowledge some technical support for WRF from Srinidhi Gadde (University of Twente), Peter Kalverla (Netherlands eScience Center), Claire Donnelly (Netherlands eScience Center), Andrea Zonato (CIMA Research Foundation) and Alberto Martilli (CIEMAT). We also thank Daniella Maiullari (Delft University of Technology) and Marjolein van Esch (Delft University of Technology) for informative early discussions of this work.

Financial support

This work is supported by the 4TU program HERITAGE (HEat Robustness in Relation To AGEing cities), funded by the High Tech for a Sustainable Future (HTSF) program of 4TU, the federation of the four technical universities in the Netherlands. This work used the Dutch national e-infrastructure with the support of the SURF Cooperative using grant no. EINF-2023.042.

References

Aksoezen, M., Daniel, M., Hassler, U., and Kohler, N.: Building age as an indicator for energy consumption, Energy Build., 87, 74–86, https://doi.org/10.1016/j.enbuild.2014.10.074, 2015.

Bahadori, E., Rezaei, F., He, B.-J., Heiranipour, M., and Attia, S.: Evaluating urban heat island mitigation strategies through coupled UHI and building energy modeling, Build. Environ., 280, 113111, https://doi.org/10.1016/j.buildenv.2025.113111, 2025.

Bechtel, B., Alexander, P. J., Beck, C., Böhner, J., Brousse, O., Ching, J., Demuzere, M., Fonte, C., Gál, T., Hidalgo, J., Hoffmann, P., Middel, A., Mills, G., Ren, C., See, L., Sismanidis, P., Verdonck, M.-L., Xu, G., and Xu, Y.: Generating WUDAPT Level 0 data – Current status of production and evaluation, Urban Clim., 27, 24–45, https://doi.org/10.1016/j.uclim.2018.10.001, 2019.

Beezley, J., Mandel, J., Farguell, A., and Chef, B.: openwfm/convert_geotiff (0.1), GitHub [code], https://github.com/openwfm/convert_geotiff (last access: 7 August 2025), 2013.

Brousse, O., Martilli, A., Foley, M., Mills, G., and Bechtel, B.: WUDAPT, an efficient land use producing data tool for mesoscale models? Integration of urban LCZ in WRF over Madrid, Urban Clim., 17, 116–134, https://doi.org/10.1016/j.uclim.2016.04.001, 2016.

Building Research Establishment: Building Research Establishment Digest: Standard U-values, Digest 108, ISBN 0 85125 285 0, Building Research Establishment, Department of the Environment, Garston Watford, 1984.

Carnieletto, L., Ferrando, M., Teso, L., Sun, K., Zhang, W., Causone, F., Romagnoni, P., Zarrella, A., and Hong, T.: Italian prototype building models for urban scale building performance simulation, Build. Environ., 192, 107590, https://doi.org/10.1016/j.buildenv.2021.107590, 2021.

Cenlin He: Update urban LCZ parameter table with more reasonable values (#1969) · wrf-model/WRF@6156b78, GitHub [code], https://github.com/wrf-model/WRF/commit/6156b78dfd350e0514d2455badcd7eab9b7d2d31 (last access: 27 March 2026), 2024.

Centraal Bureau voor de Statistiek: CBS Wijken en Buurten 2024 versie 1 WFS (v1), Nationaal Georegister [data set], https://www.nationaalgeoregister.nl/geonetwork/srv/dut/catalog.search#/metadata/ed249628-41f0-4fdd-81a8-838f7a3a8344, 2024.

Chen, F., Kusaka, H., Bornstein, R., Ching, J., Grimmond, C. S. B., Grossman-Clarke, S., Loridan, T., Manning, K. W., Martilli, A., Miao, S., Sailor, D., Salamanca, F. P., Taha, H., Tewari, M., Wang, X., Wyszogrodzki, A. A., and Zhang, C.: The integrated WRF/urban modelling system: development, evaluation, and applications to urban environmental problems, Int. J. Climatol., 31, 273–288, https://doi.org/10.1002/joc.2158, 2011.

Cheng, Y., Zhao, L., Chakraborty, T. C., Oleson, K., Demuzere, M., Liu, X., Che, Y., Liao, W., Zhou, Y., and Li, X. "Cathy": U-Surf: a global 1 km spatially continuous urban surface property dataset for kilometer-scale urban-resolving Earth system modeling, Earth Syst. Sci. Data, 17, 2147–2174, https://doi.org/10.5194/essd-17-2147-2025, 2025.

Cheval, S., Amihăesei, V.-A., Chitu, Z., Dumitrescu, A., Falcescu, V., Irașoc, A., Micu, D. M., Mihulet, E., Ontel, I., Paraschiv, M.-G., and Tudose, N. C.: A systematic review of urban heat island and heat waves research (1991–2022), Clim. Risk Manag., 44, 100603, https://doi.org/10.1016/j.crm.2024.100603, 2024.

Dang, M., van den Dobbelsteen, A., and Voskuilen, P.: A Parametric Modelling Approach for Energy Retrofitting Heritage Buildings: The Case of Amsterdam City Centre, Energies, 17, 994, https://doi.org/10.3390/en17050994, 2024.

Delft University of Technology: Residential Building Typology - NL, https://episcope.eu/building-typology/country/nl/, last access: 10 September 2024, 2014.

Demuzere, M., Bechtel, B., Middel, A., and Mills, G.: Mapping Europe into local climate zones, PLOS ONE, 14, e0214474, https://doi.org/10.1371/journal.pone.0214474, 2019.

Demuzere, M., Kittner, J., Martilli, A., Mills, G., Moede, C., Stewart, I. D., van Vliet, J., and Bechtel, B.: A global map of local climate zones to support earth system modelling and urban-scale environmental science, Earth Syst. Sci. Data, 14, 3835–3873, https://doi.org/10.5194/essd-14-3835-2022, 2022.

Demuzere, M., He, C., Martilli, A., and Zonato, A.: A hybrid 100-m global land cover dataset with Local Climate Zones for WRF (1.0.0), Zenodo [data set], https://doi.org/10.5281/zenodo.7670653, 2023a.

Demuzere, M., He, C., Martilli, A., and Zonato, A.: Technical documentation for the hybrid 100-m global land cover dataset with Local Climate Zones for WRF, https://doi.org/10.5281/zenodo.7670792, 2023b.

Foil insulation: to gap or not to gap? That is the question!: Do I need an air gap when using foil insulation, InsulationGo, https://insulationgo.co.uk/blog/do-i-need-an-air-gap-when-using-foil-insulation/, last access: 9 September 2024.

Esch, T., Brzoska, E., Dech, S., Leutner, B., Palacios-Lopez, D., Metz-Marconcini, A., Marconcini, M., Roth, A., and Zeidler, J.: World Settlement Footprint 3D - A first three-dimensional survey of the global building stock, Remote Sens. Environ., 270, 112877, https://doi.org/10.1016/j.rse.2021.112877, 2022.

Farhan, S. A., Ismail, F. I., Kiwan, O., Shafiq, N., Zain-Ahmed, A., Husna, N., and Hamid, A. I. A.: Effect of Roof Tile Colour on Heat Conduction Transfer, Roof-Top Surface Temperature and Cooling Load in Modern Residential Buildings under the Tropical Climate of Malaysia, Sustainability, 13, 4665, https://doi.org/10.3390/su13094665, 2021.

Glaudemans, R.: Een bouwhistorische waardenkaart voor de stadskern van Amsterdam [A map of architectural heritage values for Amsterdam city centre], Gemeente Amsterdam, Bureau Monumenten & Archeologie, Amsterdam, ISSN: 1875-7839, 2008.

Habib, M., Zendeli, D., van Esch, M., Timmermans, W. J., and van Ham, M.: Unsupervised clustering approach to residential typo-morphologies across multiple cities for urban heat vulnerability assessment, Sustain. Cities Soc., 137, 107107, https://doi.org/10.1016/j.scs.2025.107107, 2026.

749 Hammerberg, K., Brousse, O., Martilli, A., and Mahdavi, A.: Implications of employing detailed urban canopy
750 parameters for mesoscale climate modelling: a comparison between WUDAPT and GIS databases over Vienna,
751 Austria, Int. J. Climatol., 38, e1241–e1257, https://doi.org/10.1002/joc.5447, 2018.

752 Han, J., Mo, N., Cai, J., Ouyang, L., and Liu, Z.: Advancing the local climate zones framework: a critical review
753 of methodological progress, persisting challenges, and future research prospects, Humanit. Soc. Sci. Commun.,
754 11, 1–18, https://doi.org/10.1057/s41599-024-03072-8, 2024.

755 Havinga, L., Colenbrander, B., and Schellen, H.: Heritage attributes of post-war housing in Amsterdam, Front.
756 Archit. Res., 9, 1–19, https://doi.org/10.1016/j.foar.2019.04.002, 2020.

757 Historic England: Energy Efficiency and Historic Buildings: Insulating Early Cavity Walls,
758 https://historicengland.org.uk/images-books/publications/eehb-early-cavity-walls/heag083-early-cavity-walls/
759 (last access: 20 August 2024), 2012.

760 Huang, F., Jiang, S., Zhan, W., Bechtel, B., Liu, Z., Demuzere, M., Huang, Y., Xu, Y., Ma, L., Xia, W., Quan, J.,
761 Jiang, L., Lai, J., Wang, C., Kong, F., Du, H., Miao, S., Chen, Y., and Chen, J.: Mapping local climate zones for
762 cities: A large review, Remote Sens. Environ., 292, 113573, https://doi.org/10.1016/j.rse.2023.113573, 2023.

763 Isolatiewaarde: de Rd waarde, Rc waarde en lambdawaarde [Insulation values: the Rd value, Rc value, and lambda
764 value], https://www.isolatiemateriaal.nl/kenniscentrum/isolatiewaarde-de-rd-waarde-rc-waarde-en-
765 lambdawaarde, last access: 5 September 2024.

766 Jasińska, I., Dachowski, R., and Jaworska-Wędzińska, M.: Thermal Conductivity of Sand-Lime Products
767 Modified with Foam Glass Granulate, Materials, 14, 5678, https://doi.org/10.3390/ma14195678, 2021.

768 Kadaster: BRT TOP10NL (OGC API), PDOK [data set], ID: 576ac56d-14de-477b-a536-b430cd6ff03e,
769 https://api.pdok.nl/brt/top10nl/ogc/v1 (last access: 5 February 2025).

770 Keesjan: Isolatiemogelijkheden huis per bouwjaar [Insulation possibilities house by year of construction],
771 https://papagreen.org/wonen/isolatie/isolatiemogelijkheden-huis-per-bouwjaar/ (last access: 9 September 2024),
772 2020.

773 Kim: Rc-waarde of Rd-waarde voor isolatie – Welke waarde is goed? [Rc value or Rd value for insulation – What
774 value is good?], https://www.fabercomfortvloer.nl/blog/rc-waarde-of-rd-waarde-voor-isolatie-welke-waarde-is-
775 goed/, last access: 23 April 2024, 2022.

776 Koninklijk Verbond van Nederlandse Baksteenfabrikanten: Construeren met Metselwerk van Baksteen
777 [Constructing with Masonry from Bricks], Koninklijk Verbond van Nederlandse Baksteenfabrikanten, De Steeg,
778 https://www.knb-keramiek.nl/media/269958/brochure-construeren-met-metselwerk-van-baksteen-herziene-
779 omslag.pdf, 1999.

780 Koninklijk Verbond van Nederlandse Baksteenfabrikanten: Bouwfysische Eigenschappen en Detaillering
781 Metselwerk [Building Physics Properties and Detailing of Masonry], Koninklijk Verbond van Nederlandse
782 Baksteenfabrikanten, De Steeg, https://www.knb-keramiek.nl/media/269955/brochure-bouwfysische-
783 eigenschappen-en-detaillering-metselwerk-herziene-omslag.pdf, 2002.

784 Kuijeren, F. van: To see how your house is insulated by the year of construction,
785 https://vkmakelaars.nl/en/blog/architectural/to-see-how-your-house-is-insulated-by-the-year-of-construction/,
786 last access: 8 August 2024, 2022.

787 Kusaka, H., Kondo, H., Kikegawa, Y., and Kimura, F.: A Simple Single-Layer Urban Canopy Model For
788 Atmospheric Models: Comparison With Multi-Layer And Slab Models, Bound.-Layer Meteorol., 101, 329–358,
789 https://doi.org/https://doi.org/10.1023/A:1019207923078, 2001.

790 Li, R., Sun, T., Ghaffarian, S., Tsamados, M., and Ni, G.: GLAMOUR: GLobAl building MOrphology dataset
791 for URban hydroclimate modelling, Sci. Data, 11, 618, https://doi.org/10.1038/s41597-024-03446-2, 2024.

792 Liebregts, M. and Persoon, J.: Technische Eigenschappen van het Woningcasco in de Tijd [Technical
793 Characteristics of the Building Shell Over Time],

http://www.bouwhulparchief.nl/kennisdeling/artikelen/417_Technische_eigenschappen_van_het_woningcasco_in_de_tijd.php, 2011.

Lindenthal, T. and Johnson, E. B.: Machine Learning, Architectural Styles and Property Values, J. Real Estate Finance Econ., 71, 353–384, https://doi.org/10.1007/s11146-021-09845-1, 2025.

Maronga, B., Banzhaf, S., Burmeister, C., Esch, T., Forkel, R., Fröhlich, D., Fuka, V., Gehrke, K. F., Geletič, J., Giersch, S., Gronemeier, T., Groß, G., Heldens, W., Hellsten, A., Hoffmann, F., Inagaki, A., Kadasch, E., Kanani-Sühring, F., Ketelsen, K., Khan, B. A., Knigge, C., Knoop, H., Krč, P., Kurppa, M., Maamari, H., Matzarakis, A., Mauder, M., Pallasch, M., Pavlik, D., Pfafferott, J., Resler, J., Rissmann, S., Russo, E., Salim, M., Schrempf, M., Schwenkel, J., Seckmeyer, G., Schubert, S., Sühring, M., von Tils, R., Vollmer, L., Ward, S., Witha, B., Wurps, H., Zeidler, J., and Raasch, S.: Overview of the PALM model system 6.0, Geosci. Model Dev., 13, 1335–1372, https://doi.org/10.5194/gmd-13-1335-2020, 2020.

Martilli, A., Clappier, A., and Rotach, M. W.: An Urban Surface Exchange Parameterisation for Mesoscale Models, Bound.-Layer Meteorol., 104, 261–304, https://doi.org/10.1023/A:1016099921195, 2002.

Masson, V.: A Physically-Based Scheme For The Urban Energy Budget In Atmospheric Models, Bound.-Layer Meteorol., 94, 357–397, https://doi.org/10.1023/A:1002463829265, 2000.

Masson, V., Heldens, W., Bocher, E., Bonhomme, M., Bucher, B., Burmeister, C., de Munck, C., Esch, T., Hidalgo, J., Kanani-Sühring, F., Kwok, Y.-T., Lemonsu, A., Lévy, J.-P., Maronga, B., Pavlik, D., Petit, G., See, L., Schoetter, R., Tornay, N., Votsis, A., and Zeidler, J.: City-descriptive input data for urban climate models: Model requirements, data sources and challenges, Urban Clim., 31, 100536, https://doi.org/10.1016/j.uclim.2019.100536, 2020.

Milieu Centraal: Dakisolatie: lagere energiekosten [Roof insulation: lower energy costs], https://www.milieucentraal.nl/energie-besparen/isoleren-en-besparen/dakisolatie/, last access: 9 September 2024.

Museum Ons' Lieve Heer op Solder: Our Lord in the Attic: A Case Study - Building construction, https://www.getty.edu/conservation/publications_resources/teaching/case/olita/building/construction_building.html, last access: 9 August 2024.

Oke, T. R.: Boundary Layer Climates, 2nd ed., Routledge, United Kingdom, 464 pp., ISBN: 97811381704381987, 1987.

Oke, T. R., Mills, G., Christen, A., and Voogt, J. A.: Urban Climates, Cambridge University Press, Cambridge, https://doi.org/10.1017/9781139016476, 2017.

Oltengarm, J., van Kampen, B. J. M., Reijenga, T. H., and Drok, M.: PV system en renovatie - Een potentieel studie [PV system and renovation - A potentiality study], https://publications.tno.nl/publication/34619407/zzEymi/2001-G&I-R0067.pdf, 2001.

Orsel, E.: Brickwork in Leiden: a Survey of Sixteenth and Seventeenth-Century Characteristics, in: Proceedings of The Second International Congress on Construction History, Queens' College, Cambridge University 29th March–2nd April, The Second International Congress on Construction History, Queens' College, 2379–2394, ISBN 0701702052, 2006.

van Overveld, M., van der Graaf, P. J., Eggink-Eilander, S., and Berghuis, M. I.: Praktijkboek Bouwbesluit 2012, [Practical Guide to Building Regulation 2012], ISBN: 9789012134248, 2011.

Pappaccogli, G., Giovannini, L., Cappelletti, F., and Zardi, D.: Challenges in the application of a WRF/Urban-TRNSYS model chain for estimating the cooling demand of buildings: A case study in Bolzano (Italy), Sci. Technol. Built Environ., 24, 529–544, https://doi.org/10.1080/23744731.2018.1447214, 2018.

Pappaccogli, G., Giovannini, L., Zardi, D., and Martilli, A.: Assessing the Ability of WRF-BEP + BEM in Reproducing the Wintertime Building Energy Consumption of an Italian Alpine City, J. Geophys. Res. Atmos., 126, e2020JD033652, https://doi.org/10.1029/2020JD033652, 2021.

Patel, P. and Roth, M.: A High-Resolution Dataset of Global Urban Fraction for Mesoscale Urban Modelling (2.0.1), Zenodo [data set], https://doi.org/https://doi.org/10.5281/zenodo.7298393, 2022.

Peters, R., Dukai, B., Vitalis, S., Van Liempt, J., and Stoter, J.: Automated 3D Reconstruction of LoD2 and LoD1 Models for All 10 Million Buildings of the Netherlands, Photogramm. Eng. Remote Sens., 88, 165–170, https://doi.org/10.14358/PERS.21-00032R2, 2022.

Pisello, A. L., Pignatta, G., Castaldo, V. L., and Cotana, F.: Experimental Analysis of Natural Gravel Covering as Cool Roofing and Cool Pavement, Sustainability, 6, 4706–4722, https://doi.org/10.3390/su6084706, 2014.

Quach, T.: opengeoshub/becagis (24.11.6), GitHub [code], https://github.com/opengeoshub/becagis (last access: 18 June 2025), 2024.

Rasooli, A.: In-Situ Determination of Buildings' Thermo- Physical Characteristics: Method Development, Experimentation, and Computation, ABE Archit. Built Environ., 1–228, https://doi.org/10.7480/abe.2020.07.4989, 2020.

Rijksdienst voor het Cultureel Erfgoed: Spouwmuren [Cavity walls], https://kennis.cultureelerfgoed.nl/index.php/Spouwmuren, last access: 12 August 2024.

Rijksdienst voor Ondernemend Nederland: Voorbeeldwoningen 2022 | bestaande bouw [Reference dwellings 2022 | existing buildings], Publication number: RVO-231-2022/BR-DUZA, https://www.rvo.nl/sites/default/files/2023-01/brochure-voorbeeldwoningen-bestaande-bouw-2022.pdf, 2022.

Rob: Wat Is Een Spouwmuur? [What is a cavity wall?], Grimbergen Isolatietechniek, https://grimbergenisolatie.nl/wat-is-een-spouwmuur/, last access: 15 August 2024, 2023.

Ronda, R. J., Steeneveld, G. J., Heusinkveld, B. G., Attema, J. J., and Holtslag, A. a. M.: Urban Finescale Forecasting Reveals Weather Conditions with Unprecedented Detail, Bull. Am. Meteorol. Soc., 98, 2675–2688, https://doi.org/10.1175/BAMS-D-16-0297.1, 2017.

Salamanca, F., Krpo, A., Martilli, A., and Clappier, A.: A new building energy model coupled with an urban canopy parameterization for urban climate simulations—part I. formulation, verification, and sensitivity analysis of the model, Theor. Appl. Climatol., 99, 331–344, https://doi.org/10.1007/s00704-009-0142-9, 2010.

Sandvik, B., Milošević, D., and Steeneveld, G.-J.: Data supporting the publication: Mapping urban fabric for enhanced urban climate modelling based on a historical building classification, https://doi.org/10.4121/8687610f-a25e-49ca-adc6-8bcce0f5a22b, 2026.

Scottish Government: U-value: guidance, https://www.gov.scot/publications/tables-of-u-values-and-thermal-conductivity/, 2020.

Stewart, I. D. and Oke, T. R.: Local Climate Zones for Urban Temperature Studies, Bull. Am. Meteorol. Soc., 93, 1879–1900, https://doi.org/10.1175/BAMS-D-11-00019.1, 2012.

Table 6 Thermal Conductivity, Specific Heat Capacity and Density, https://help.iesve.com/ve2021/table_6_thermal_conductivity__specific_heat_capacity_and_density.htm, last access: 16 August 2024, 2021.

Table 15 Thermal Resistances of Air Gaps, https://help.iesve.com/ve2021/table_15_thermal_resistances_of_air_gaps.htm, last access: 16 August 2024, 2021.

TABULA Project Team: Typology Approach for Building Stock Energy Assessment. Main Results of the TABULA project, Institut Wohnen und Umwelt GmbH, Darmstadt, https://episcope.eu/fileadmin/tabula/public/docs/report/TABULA_FinalReport.pdf, 2012.

The Engineering Toolbox: Emissivity Coefficients of Common Materials: Data & Reference Guide, https://www.engineeringtoolbox.com/emissivity-coefficients-d_447.html, last access: 14 August 2024, 2003a.

The Engineering Toolbox: Specific Heat of Common Materials – Engineering Reference, https://www.engineeringtoolbox.com/specific-heat-capacity-d_391.html, last access: 14 August 2024, 2003b.

Tornay, N., Schoetter, R., Bonhomme, M., Faraut, S., and Masson, V.: GENIUS: A methodology to define a detailed description of buildings for urban climate and building energy consumption simulations, Urban Clim., 20, 75–93, https://doi.org/10.1016/j.uclim.2017.03.002, 2017.

Tussenbroek, G. V.: The great rebuilding of Amsterdam (1521–1578), Urban Hist., 46, 419–442, https://doi.org/10.1017/S0963926818000561, 2019.

Van de Voorde, S., Bertels, I., and Wouters, I.: Post-war building materials in housing in Brussels 1945-1975 / Naoorlogse bouwmaterialen in woningen in Brussel 1945-1975 / Matériaux de construction d'après-guerre dans l'habitation à Bruxelles 1945-1975, Graphius Group, Gent, ISBN 978-94-91912-04-7, 2015.

Vekemans, H.: Legislation and Brickwork Facades in A Historical Perspective 1900-2015, in: Brick : an exacting material, edited by: Wingender, J. P., Architectura & Natura, Amsterdam, 135–148, ISBN 978-94-6140-027-7, 2016.

de Vree, J.: warmtegeleidings-coëfficiënt (lambda) [thermal conductivity coefficient (lambda)], https://www.joostdevree.nl/w/warmtegeleidingscoefficient?highlight=WyJsYW1iZGEiXQ==, last access: 22 September 2026, 2026.

Weather Research and Forecasting Model, GitHub [code], https://github.com/wrf-model, last access: 5 November 2026., 2026.

Zhu, X. X., Qiu, C., Hu, J., Shi, Y., Wang, Y., Schmitt, M., and Taubenböck, H.: The urban morphology on our planet – Global perspectives from space, Remote Sens. Environ., 269, 112794, https://doi.org/10.1016/j.rse.2021.112794, 2022.

Zonato, A., Martilli, A., Di Sabatino, S., Zardi, D., and Giovannini, L.: Evaluating the performance of a novel WUDAPT averaging technique to define urban morphology with mesoscale models, Urban Clim., 31, 100584, https://doi.org/10.1016/j.uclim.2020.100584, 2020.